Innovations in craniofacial bone and periodontal tissue engineering – from electrospinning to converged biofabrication

Zeynep Aytac, Nileshkumar Dubey, Arwa Daghrery, Jessica A. Ferreira, Isaac J. de Souza Araújo, Miguel Castilho, Jos Malda & Marco C. Bottino

I·M3
Institute of Materials,
Minerals & Mining

ASM INTERNATIONAL

Taylor & Francis
Taylor & Francis Group

Check for updates

FULL CRITICAL REVIEW

Innovations in craniofacial bone and periodontal tissue engineering – from electrospinning to converged biofabrication

Zeynep Aytac [a]*†, Nileshkumar Dubey [a]†, Arwa Daghrery [a], Jessica A. Ferreira [a], Isaac J. de Souza Araújo [a], Miguel Castilho [b,c,d], Jos Malda [b,c,e] and Marco C. Bottino [a,f]

aDepartment of Cariology, Restorative Sciences, and Endodontics, University of Michigan, School of Dentistry, Ann Arbor, MI, USA; bRegenerative Medicine Center, University Medical Center Utrecht, Utrecht, The Netherlands; cDepartment of Orthopedics, University Medical Center Utrecht, Utrecht, The Netherlands; dDepartment of Biomedical Engineering, Eindhoven University of Technology, Eindhoven, The Netherlands; eDepartment of Clinical Sciences, Faculty of Veterinary Medicine, Utrecht University, Utrecht, The Netherlands; fDepartment of Biomedical Engineering, College of Engineering, University of Michigan, Ann Arbor, MI, USA

ABSTRACT
From a materials perspective, the pillars for the development of clinically translatable scaffold-based strategies for craniomaxillofacial (CMF) bone and periodontal regeneration have included electrospinning and 3D printing (biofabrication) technologies. Here, we offer a detailed analysis of the latest innovations in 3D (bio)printing strategies for CMF bone and periodontal regeneration and provide future directions envisioning the development of advanced 3D architectures for successful clinical translation. First, the principles of electrospinning applied to the generation of biodegradable scaffolds are discussed. Next, we present on extrusion-based 3D printing technologies with a focus on creating scaffolds with improved regenerative capacity. In addition, we offer a critical appraisal on 3D (bio)printing and multitechnology convergence to enable the reconstruction of CMF bones and periodontal tissues. As a future outlook, we highlight future directions associated with the utilisation of complementary biomaterials and (bio)fabrication technologies for effective translation of personalised and functional scaffolds into the clinics.

Introduction

Successful and predictable reconstruction of craniomaxillofacial (CMF) bones due to congenital malformations, trauma, infection, tumour resection and sport injuries remains a major clinical challenge due to the presence of sensory organs, high vasculature density, and differences in skeletal tissue characteristics [1]. Moreover, severe damage to CMF bones can impair breathing, listening, chewing and speech abilities, along with a person's esthetic features, which can lead to enduring psychological problems and poor self-esteem [2,3]. Noteworthy, the management of CMF injuries is especially problematic as clinicians need to monitor bacterial infection in extremely vulnerable areas, such as the oral microenvironment [4].

Some of the most prevalent pathologies that affect our oral health include tooth decay, gum disease (i.e. periodontitis), and oral cancer [5]. Periodontitis, a chronic inflammatory disease that results in the loss of alveolar bone and other key tooth-supporting structures (gingiva, periodontal ligament, and cementum), affects more than 45% of the US adult population [6,7]. It is described by the gradual destruction of periodontal tissues, which if left untreated, it may lead to

tooth loss [8]. Hence, the ultimate goal of periodontal tissue engineering has been not only the restoration of alveolar bone, but the simultaneous reestablishment of functionally oriented periodontal ligament (PDL) fibres firmly attached to the regenerated cementum and bone (Figure 1), thus extending the lifespan of the natural dentition.

Clinically speaking, the management of periodontitis demands a series of procedures that involves scaling and root planning, in addition to, in some instances, the systemic (oral) administration of antibiotics. Nonetheless, limited periodontal tissue regeneration results from this strategy [9]. Meanwhile, the use of autologous (e.g. iliac crest) bone grafts has been largely employed for alveolar bone reconstruction; however, this approach brings major concerns regarding the need for multiple surgeries, associated morbidity, and a number of possible complications, including the infection of the operated area [10]. Importantly, from a clinical standpoint, it is particularly difficult to shape and conform natural or synthetic bone grafts into the complex three-dimensional (3D) architecture of periodontal defects. Furthermore, bone grafts may only fill osseous defects and work inadequately in
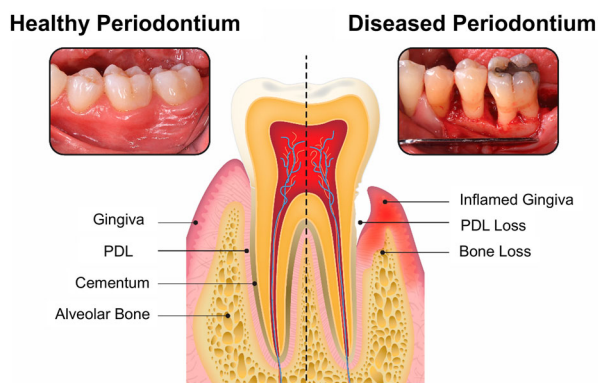
Figure 1. Schematic illustrations showing a longitudinal section through dento-gingival part of a tooth and tooth supporting structures between healthy and diseased periodontium. In particular, as the disease progresses, the periodontal complex (bone, gingiva, periodontal ligament [PDL], and cementum) is gradually destroyed and progress along the tooth root creating a deepening pocket.

supporting true physiological regeneration of the multiple periodontal tissues [11]. Remarkably, recent strides in tissue engineering in addition to the rapidly evolving field of biofabrication have not only improved clinical outcomes of regenerative therapies, but have also set new hopes for the effective translation of personalised and more predictable strategies for bone and periodontal regeneration [12–15]. Nonetheless, over the last few decades, among the clinically available techniques, guided tissue regeneration (GTR) and guided bone regeneration (GBR) have invariably been the most practical approaches to manage and clinically treat the tissue destruction provoked by periodontitis [16,17].

Guided tissue and guided bone regeneration (GTR/GBR) are defined as dental surgical procedures aimed at regenerating lost periodontal structures to change the prognosis of a tooth from 'questionable' to 'favourable', and thus ameliorate oral health-related quality of life for millions of patients worldwide. Briefly, in these procedures, a barrier membrane is used to avert soft tissue migration into the bone defect while providing space maintenance, wound stabilisation, and, ultimately, a sheltered niche for resident progenitor cells situated in the residual PDL, contiguous alveolar bone, or blood to recolonise the root area and differentiate into a new periodontal supporting apparatus [8,18].

Classically, GTR/GBR membranes are divided into two groups: non-resorbable and resorbable. Non-resorbable membranes are mostly polytetrafluoroethylene-based (PTFE), such as high-density PTFE and titanium-reinforced high-density PTFE [19]. Although non-resorbable materials are biocompatible and have led to positive clinical outcomes, they are biologically inert and exert only a physical barrier function. Moreover, their use demands a second surgery for its removal, which leads to added discomfort and increases the risk of infection. In this way, a

variety of resorbable materials were developed as an alternative to non-resorbable options [16,19]. Resorbable membranes can be synthesised from either natural, synthetic, or blends of synthetic and natural polymers [19,20]. However, the well-known and intrinsic drawbacks in existing membranes, such as low attachment to adjacent tissues, lack of curative properties, and reduced regenerative capacity have propelled the field in the direction of resorbable and multifunctional polymeric membranes with controlled degradation rate, mechanical competence, and multiple therapeutic properties as to eradicate infection, ablate inflammation, and support tissue regeneration.

From a broad tissue engineering perspective, the pillars for the development of clinically translatable scaffold-based strategies for craniofacial bone and periodontal tissue regeneration have primarily included electrospinning and 3D printing technologies (Figure 2). In the last two decades, electrospinning has become of great importance due to its simplicity and the possibility of employing a wide range of degradable polymers in the fabrication of GTR/GBR membranes and scaffolds for periodontal regeneration [21,22]. Moreover, the integration of biologically active molecules (e.g. growth factors) and therapeutic compounds [23,24], such as bioceramics and metal oxides nano/microparticles, have led to encouraging regenerative outcomes [17,25,26]. Despite the tremendous advantages associated with electrospun membranes, true physiological regeneration of the periodontium still embodies one of the greatest challenges in regenerative periodontics, not only because of the varying degrees of tissue destruction produced by the disease, but more importantly due to the highly complex, 3D periodontal tissue architecture and multiplicity of tissues involved that need to be reconstructed. Accordingly, the creation of defect-specific scaffolds to recapitulate the native tissues and the carefully designed structure of the periodontium is paramount for predictable regeneration of both soft (gingiva and periodontal ligament) and hard (alveolar bone and cementum) periodontal tissues.

3D printing, an additive manufacturing process in which a membrane or scaffold can be fabricated in a layer-by-layer fashion to obtain defect-specific and anatomically complex constructs, has been deemed a paradigm shifting enabling technology in regenerative dentistry [11,27,28]. Currently, 3D printing strategies involve designing mono- or multiphasic scaffolds presenting macro- (scaffold structure), micro- (pore size for bone zone and fibre alignment for PDL zone), and nano-scale (surface topography) features to guide the coordinated growth and regeneration of the distinct periodontal tissues [11,12,29,30]. Notably, periodontal-related cell types can be 3D bioprinted, and thus distributed at specific locations of
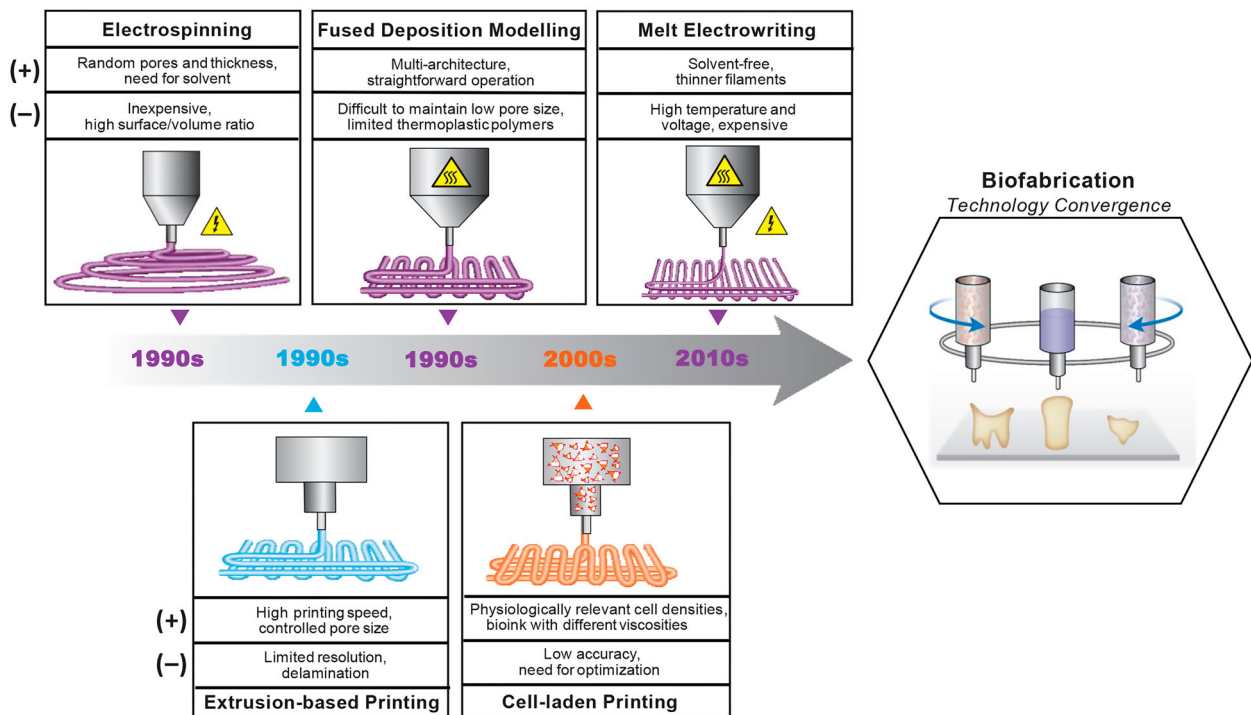
Figure 2. Timeline of the development of electrospinning and extrusion-based 3D printing technologies for the generation of regenerative bone and periodontal constructs, their advantages (+) and dis-advantages (–), and outlook towards the convergence of these technologies.

anatomically defined scaffolds to promote the coordinated growth and simultaneous regeneration of soft and hard periodontal tissues [13,31,32].

Biofabrication is a rapidly evolving field that uses 3D printing methods to engineer biologically functional and highly organised structures primarily using biomaterials and cells. In recent years, among the various tools within the biofabrication armamentarium, particularly pertaining to 3D printing and bioprinting (i.e. cell-laden scaffolds) techniques, much focus has been given to extrusion-driven processes, which even though are technologically more simple compared to other printing methods, they allow for successful processing of a wide range of cell-free or cell-laden scaffolds with significant translational potential for bone and periodontal regeneration [33–35]. Succinctly put, extrusion-based printing can be classified into two major subgroups: thermal and non-thermal extrusion 3D printing. Remarkably, the latest extrusion-based technologies have also explored the benefits of coaxial and multimaterial printing to fabricate patient-specific implants mimicking complex tissue interfaces (e.g. bone-PDL, bone-cartilage, bone-ligament, etc.), which has been challenging to recapitulate using conventional scaffold fabrication methods [36,37]. A promising approach in interface tissue engineering lies in the merging of electro-driven fabrication tools with extrusion-based printing into a single fabrication platform. More specifically, the combination of solution/melt electrospinning or melt electrowriting with extrusion of cell-laden hydrogels, has

shown to appreciably enhance the mechanical competence of cell-laden hydrogels while enabling spatial distribution of different cell types [38,39]. Overall, the combination of complementary fabrication technologies into a single platform opens up limitless and forward-thinking opportunities for engineering functional interface tissues by better resembling the mechanical and biological gradients observed in native tissue interfaces [40].

In this review, we offer an analytical appraisal of the newest innovations in 3D printing and bioprinting strategies for craniofacial bone and periodontal tissue regeneration and set directions in devising highly complex 3D architectures for successful translation of personalised scaffolds for regenerative dentistry. In the first part, the principles of electrospinning applied to the generation of biodegradable nanofibrous polymeric scaffolds for use as GTR/GBR barrier membranes, as well as, tissue scaffolds for bone and periodontal tissue engineering are discussed. The second part carefully elaborates on different types of extrusion-based 3D printing technologies with a focus on how distinct biomaterial classes can be modified or functionalised to engineer scaffolds with improved regenerative capacity. This includes recent work on extrusion-based bioprinting to render cell-laden scaffolds with controlled geometry, architecture, and biological features to develop functional living tissues/organs. Next, we provide a critical assessment on the latest innovations in 3D printing and multitechnology fabrication process to enable the generation

of gradient and anatomically complex structures to allow the functional reconstruction of the alveolar bone-PDL interface and patient-specific periodontal defects. Finally, as a future outlook, we highlight upcoming directions associated with the utilisation of complementary biomaterials and (bio)fabrication technologies for effective translation of personalised and functional scaffolds for predictable reconstruction of CMF bones and periodontal tissues.
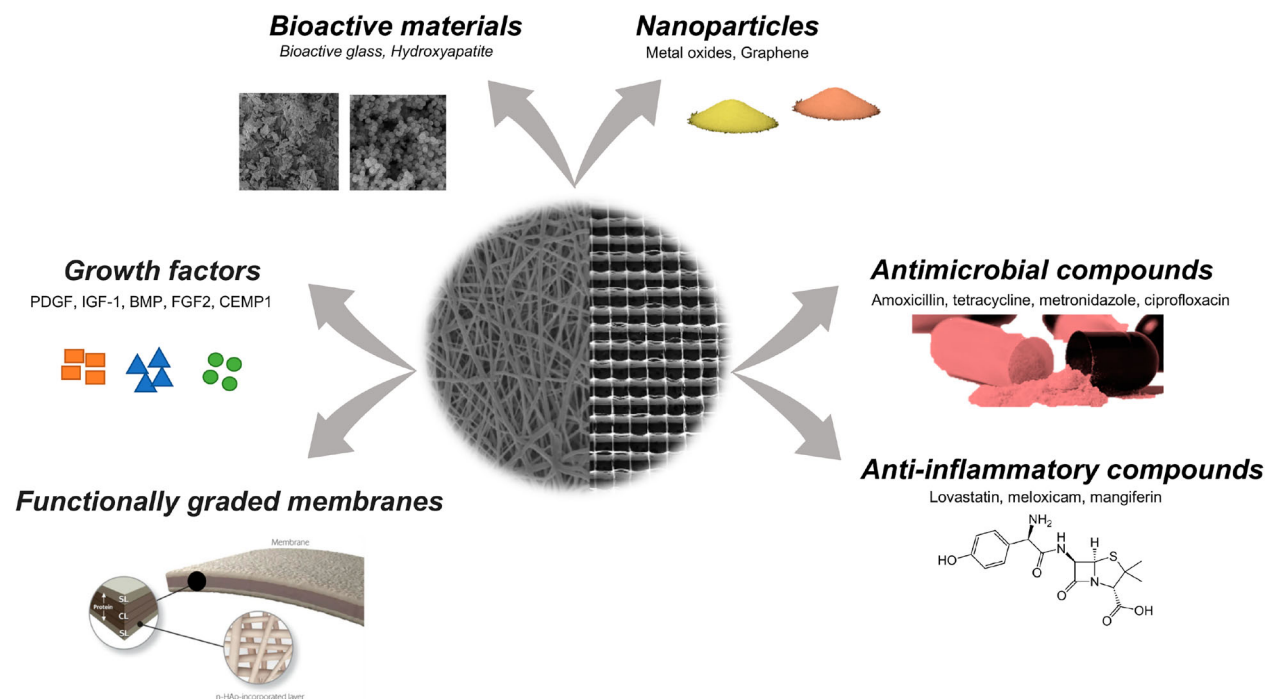
Electrospinning

A wide range of scaffold-based tissue engineering techniques and materials have been developed for regeneration of impaired periodontal tissues. Over the last decade, researchers have focused on methods such as casting, dynamic filtration, and electrospinning to generate biodegradable polymeric membranes for periodontal tissue regeneration [16,41]. Among them, electrospinning, a versatile and easy to use technique, has been widely explored to produce extracellular matrix (ECM)-mimicking nanofibrous scaffolds [22] with or without the incorporation of a vast array of therapeutics for infection eradication, inflammation control, and to further boost tissue regeneration (Figure 3).

Traditionally, the electrospinning setup has three major components, namely a syringe filled with a polymer solution and capped with a metallic needle, a high voltage supply, and a grounded collector positioned at a predetermined distance from the tip of the needle. The solution is charged by an optimised voltage while it flows through the needle and forms the so-called Taylor cone when the induced potential difference overcomes the surface tension of the polymer solution being dispensed [42,43]. While travelling through the air, the polymer jet experiences instabilities and as the solvent evaporates fibres solidify and are deposited on the collector [43]. Electrospinning enables the fabrication of random, aligned, or core–shell micro/nanofibres when using coaxial needle configurations. Electrospun fibres possess a high surface-to-volume ratio and allow the encapsulation and/or decoration with biomolecules [43,44], thus contributing to the generation of single (monophasic) or multilayered (multiphasic), functionally graded or not, scaffolds with therapeutic properties and tremendous impact on dental, oral, and craniofacial tissue regeneration (Table 1) [16,45].

Monophasic electrospun membranes with therapeutic properties

Membranes for GTR/GBR are among the most positive methods to treat the destruction caused by periodontitis; as they provide enough time for resident progenitor cells to populate the affected area while excluding epithelial/connective tissue cells from the periodontal defect. However, the regeneration of periodontal tissues might be thwarted without proper mechanisms to control and ultimately eradicate infection [16,42]. With this in mind, antimicrobial-releasing electrospun fibres have been engineered as an alternative to systemically administered antibiotics to promote localised bacterial load reduction in the periodontal defect. Most of the published studies report the use of metronidazole

Figure 3. Schematic representation of chemical and physical functionalisation of (melt-)electrospun fibres for bone and periodontal tissue regeneration. Adapted from [42].

Table 1. Selected references on electrospinning for tissue engineering strategies in periodontal tissue regeneration

Reference	Advantages/disadvantages	Most relevant findings
Monophasic electrospun membranes		
[46]	(+) biodegradable, nano-size diameter	Good osteoinductive ability as a result of the characteristics of nHA.
[47]	(+) various types of synthetic polymers can be used to form fibres	High potential for osteoconduction and mineralisation of ECM with PLLA membranes and better osteoinductivity with pisPLLA membranes.
[48]	(+) readily functionalised with bioactive molecules	Increased proliferation of preosteoblasts as compared to Epiguide and membranes without BG.
[49]	(+) fibres can also be produced from natural polymers	Enhanced osteogenic gene expression; able to promote periodontal tissue regeneration in the furcation defect of dogs.
[50]	(+) biodegradable, two types of antibiotics were incorporated into nanofibres	Prolonged release of MET and CIP and significant inhibition growth of bacteria with CIP including nanofibres.
[51]	(–) requirement of additional step to prevent the burst release of hydrophilic drug (CIP HCl)	Controlled release of CIP from nanofibres. thanks to antimicrobial oligomer developed.
[52]	(+) blending with gelatin improved stretching ability of membranes under wet conditions	Antibacterial activity against periodontopathogens.
[53]	(–) burst release depending on nHA content	Slow release of AMX, and biomineralisation owing to nHA
[54]	(–) burst release of MX	Achieved prolonged drug release, high proliferation rate.
[55]	(+) aligned and random fibre production	Proliferation and osteogenic differentiation of stem cells, sustained release of DEX thanks to aligned fibres.
Coaxial nano/microfibrous electrospun membranes		
[56]	(+) sustained release of hydrophilic drug (–) complex process of coaxial fibre production	Controlled release of TET-HCl for 75 days for periodontal regeneration.
[57]	(+) release behaviour might be tuned by core:shell flow ratio	The release as sustained over 4 days.
[58]	(+) maintaining bioactivity of GFs (+) incorporation of different bioactive agents in core and shell	Bone regeneration was improved by 43% compared with single systems.
[59]	(+) protecting sensitive GFs from toxic solvents used (–) complex process of coaxial fibre production	Osteoconductivity and osteoinductivity can be modified due to the sustained release of factors loaded.
Multiphasic and functionally graded electrospun membranes		
[60]	(+) straightforward production compared to coaxial electrospinning	Sustained release were achieved for 28 days and regeneration of alveolar ridge was improved.
[42]	(+) the multiphasic and most advanced constructs achieved by electrospinning	nHA and MET provides the osteoinductivity and antibacterial activity to the membrane for periodontal regeneration, respectively.

(MET) as the medicament of choice [57,60–62]. For instance, MET-releasing polymeric fibres were able to inhibit the growth of known periodontopathogens (e.g. *Porphyromonas gingivalis*) [61]. In addition, other researchers addressed the potential of equally important antibiotics, such as tetracyclines [56,63,64] and ciprofloxacin [50,51] and stated similar antimicrobial outcomes – attesting for the versatility of polymeric electrospun fibres as drug delivery systems for periodontal infection ablation [50].

As previously highlighted, the modification of electrospun polymeric scaffolds with a wide variety of metal oxides as means to impair multifunctionality have been pursued [52]. Interestingly, in a recent study, zinc oxide (ZnO)-doped poly(ε-caprolactone) nanofibres displayed not only antimicrobial activity (Figure 4(a)), but more importantly led to the upregulation (*in vitro*) of bone-related genes and reduced the size of an osseous defect *in vivo* (Figure 4(b,c)) [65]. Electrospinning was used to generate branched-shaped ZnO-doped PCL membranes. The unique fibre morphology, similar to a rose stem, led to antimicrobial effects against *Pseudomonas aeruginosa*, improved the membranes' strength, and did not compromise epithelial cells' attachment or viability. Moreover, the unique rose stem-like fibre morphology enhanced adhesion to soft tissue, which, in combination with bacterial inhibition, suggests that these scaffolds could be an interesting approach for regenerative strategies in CMF sites prone to infections

[66]. Meanwhile, alternative strategies have also focused on the combination of antimicrobial agents with bioceramics [53,54]. For instance, PCL fibres loaded with hydroxyapatite (HAp) particles and amoxicillin (AMX) led to mineral precipitation, controlled drug release, and antimicrobial action [53]. Similarly, to afford anti-inflammatory properties and induce bone formation, chitosan, polyvinyl alcohol, and HAp-based composite membranes containing meloxicam (MX) were also reported [54]. Altogether, the aforementioned strategies prove the opportunities associated with the electrospinning technique for the development of tissue-specific scaffolds with drug delivery abilities. Nonetheless, one should bear in mind that, incorporation of antimicrobial and regenerative therapeutics often demands systematic screening on their mechanisms of action to provide the most beneficial synergistic effect.

Since the early 2000s, electrospun membranes have been developed for periodontal tissue engineering. Calcium phosphate (CaP)-based ceramics have been widely used as bioactive inorganic materials in electrospun membranes for GTR/GBR applications [17,46,47,67–69]. For instance, the incorporation of nano-hydroxyapatite (nHAp) particles into PCL led to cytocompatible fibres capable to induce mineral precipitation and stimulate osteoblast-like cells to upregulate the expression of an early marker of osteogenic differentiation (alkaline phosphatase) [17]. Similarly, type I collagen/PCL nanofibres doped with HAp
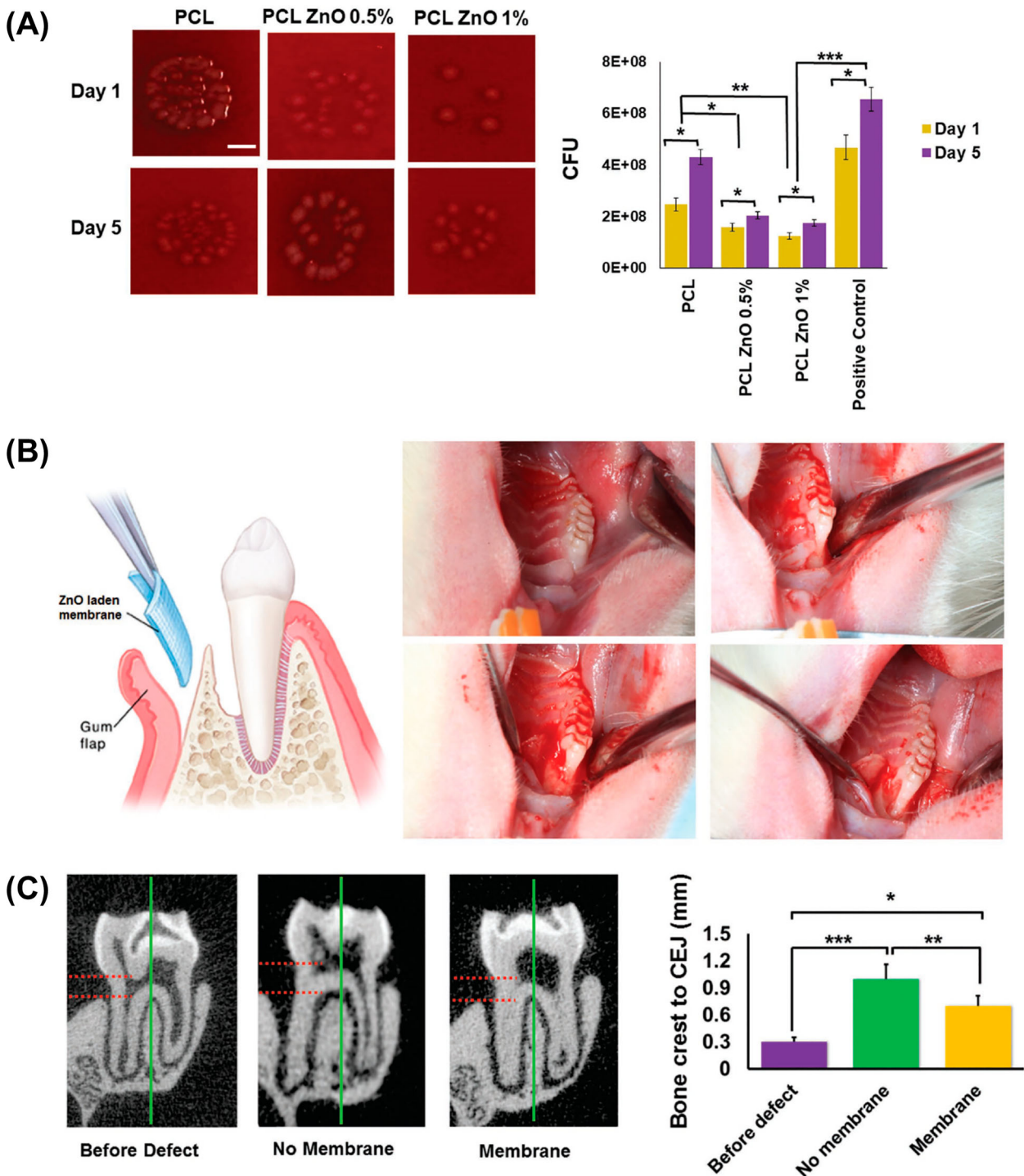
Figure 4. (a) Colony forming unit (CFU) qualitative and quantitative characterisation of the antimicrobial properties of PCL engineered membranes containing different concentrations of ZnO nanoparticles. (b) Rat periodontal defect model depicting the surgical procedure and placement of membrane, and (c) Micro-CT analysis and semi-quantitative measurements (in mm) from the bone crest to the cemento-enamel junction (CEJ) at each time interval, before and after defect, as well as after the membrane implantation. Adapted from [65].

favourably supported periodontal ligament cells proliferation and upregulated osteogenic-related gene expression [46]. Alternative biodegradable polymers, such as poly-L-lactic acid or poly(isosorbide succinate-co-L-lactide) have also been successfully blended with collagen and HAp leading to favourable regenerative outcomes [47]. The effects associated with the use of bioactive glasses (BGs) have also been demonstrated [48,49]. Composite electrospun membranes consisting of collagen, chitosan, and BG were shown to favour osteogenic gene expression, antimicrobial action, and *in vivo* periodontal tissue regeneration in a clinically relevant Class II furcation defect model [49]. Another study [55] revealed that the incorporation of a magnesium silicate (fosterite) enhanced the therapeutic potential of dexamethasone (DEX) to stimulate osteogenic differentiation of stem cells from human exfoliated deciduous teeth [55].

Concerning the well-established value of DEX as an osteogenic factor, in a recent study from our group, poly(lactic-co-glycolic acid) (PLGA) electrospun nanofibres were loaded with DEX-β-cyclodextrin inclusion complex (DEX-β-CD) based on the ability of β-CD to improve the solubility and control the release of lipophilic drugs [70]. PLGA/DEX-β-CD nanofibrous membranes demonstrated a sustained release of DEX and stimulated dental pulp stem cells to express important osteogenic markers with promising potential for bone tissue regeneration [70].

An interesting approach was recently reported using gelatin methacryloyl hydrogel (GelMA) to fabricate CaP-doped electrospun fibres to mimic the periosteum structure, and thus hasten bone regeneration [71]. GelMA/CaP electrospun fibres exhibited superior bioactivity when immersed in simulated body fluid (SBF), induced mineralisation of pre-osteoblasts, and led to a vasculogenic response of endothelial cells. Altogether, these outcomes reinforce the possibilities of devising hybrid biomaterials to mimic the synergistic activity between organic and inorganic components of native bone and periodontal tissues [71].

To further improve their biofunctionality, growth factors (GFs) have been added to electrospun membranes and scaffolds [23,58,59,72]. Growth factors are natural proteins that modulate cellular functions, such as proliferation, migration, differentiation, and the formation of extracellular matrix (ECM). In a study by Chen et al. [23], poly(ethylene glycol) (PEG)-stabilised amorphous calcium phosphate (ACP) nanoparticles containing recombinant human cementum protein 1 (rhCEMP1) were formulated and then utilised to fabricate, via electrospinning, multiphasic scaffolds constituted of PCL, type I collagen, and rhCEMP1/ACP [23]. From a regenerative standpoint, the engineered scaffold, when evaluated in a relevant *in vivo* periodontal defect model, led to cementum-like tissue formation after 8 weeks, thus supporting the ability of tissue regeneration when proper molecules are encapsulated into nanofibres [23]. Nonetheless, GFs are sensitive molecules and caution needs to be exercised in the electrospinning process to maintain their bioactive profile [16].

Coaxial nano/microfibrous electrospun membranes

Coaxial electrospinning consists of two separate solutions that form core–shell fibres, where the core and shell portions can house distinct therapeutic cargos, especially when aiming at defined spatiotemporal release patterns based on the regenerative goal. For instance, by using coaxial electrospinning, it is feasible to have an osteoinductive molecule loaded within the core and an antimicrobial medication in the shell [57,62]. The aforesaid arrangement is of significant relevance in periodontal regeneration once the outer layer (shell) containing the antimicrobial drug releases first to help eradicate infection, while the osteoinductive molecule in the inner layer (core), leaches out at a later stage, thus stimulating new tissue formation in an infection-free environment. Moreover, as previously alluded, coaxial electrospinning can also be used to shelter sensitive molecules from organic and harsh solvents commonly used to obtain polymeric solutions that would negatively affect their bioactivity before nanofibres' production.

It is well-established that the regeneration of bone tissue is controlled by both osteogenic and angiogenic GFs, which are expressed in a synchronised fashion. An elegant demonstration of the opportunities involved in the creation of controlled co-delivery of growth factors through core–shell nanofibres has been recently reported. Cheng et al. [58] used a dual growth factor-release system to achieve time-controlled of GFs release to amplify vascularised bone regeneration. In that study, core–shell nanofibrous scaffolds were fabricated using coaxial electrospinning and layer-by-layer (LBL) techniques, where bone morphogenetic protein 2 (BMP2) was loaded into the core of the nanofibres and connective tissue growth factor (CTGF) was attached onto the surface (Figure 5(a–d)). The findings confirmed the sustained release of BMP2 and a rapid release of CTGF. Importantly, *in vitro* and *in vivo* data showed improvements in bone regeneration when the dual-drug release system was used (Figure 5(e)) [58]. Even though the literature emphasised the relevance of bioactive molecules (e.g. growth factors) for bone regeneration and the well-understood involvement of these biological cues in a plethora of regenerative approaches, the need for a suitable carrier is essential to guarantee their efficacy [16,43,44]. Due to the low stability of these molecules and their inactivation by other proteins in physiologic conditions, scaffold-based bioinspired immobilisation mechanisms have been conceived to control release profiles and specific targets of GFs in regenerative strategies [73]. Therefore, these scaffolds and controlled mechanisms of release may help to surpass the challenges involved with the use of bioactive molecules and bring the possibility of translating laboratory research into practice [73,74].

Multiphasic and functionally graded electrospun membranes

Although single layer membranes and scaffolds, created by conventional and/or coaxial electrospinning, present notable advantages and translational potential with fibre diameters close to the ones found in the ECM of native tissues, they do not provide perfect hierarchical organisation and spatial gradient found in living tissues. In periodontal tissue regeneration,
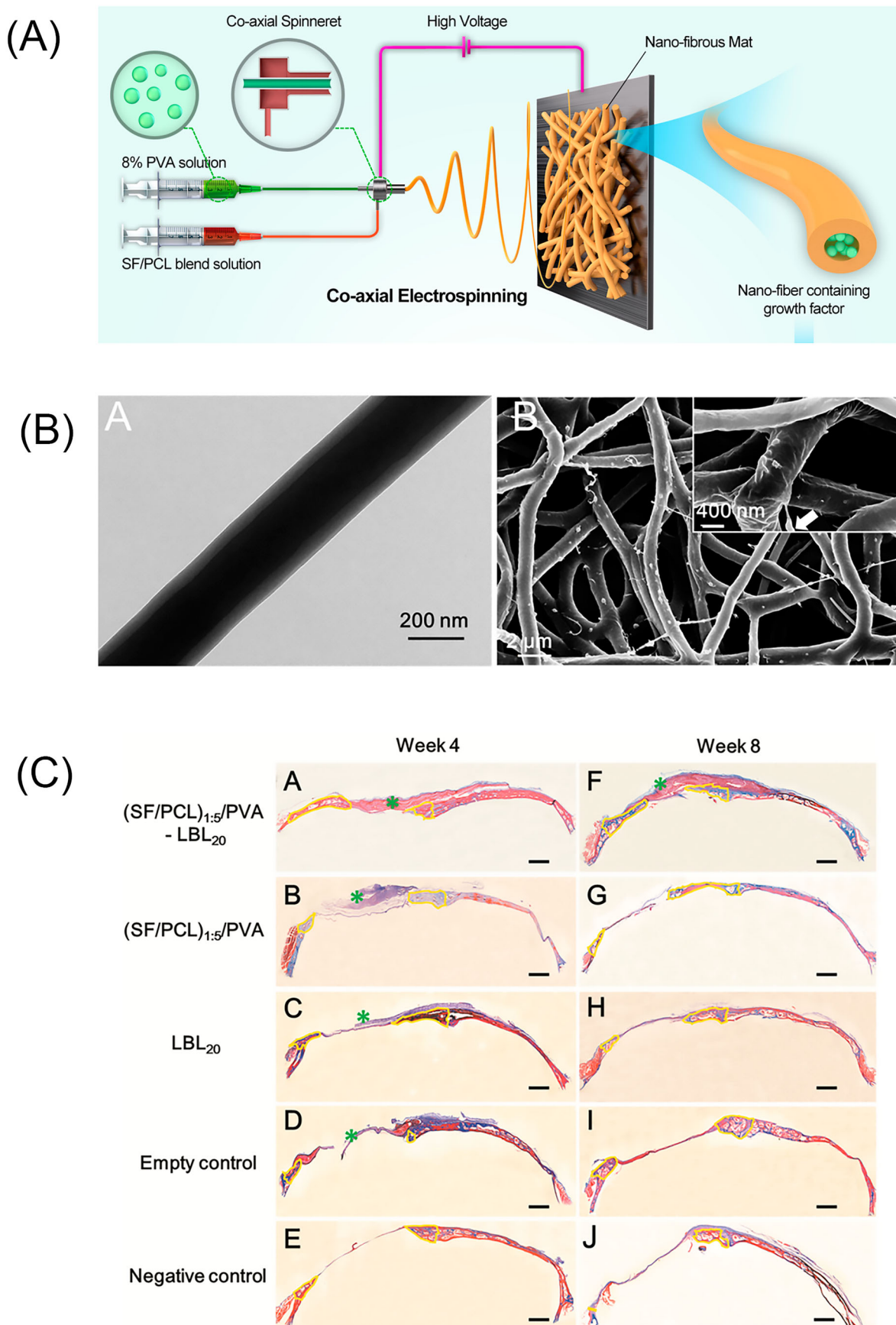
Figure 5. (a) Schematic illustration of the Co-axial electrospinning, (b) TEM (A) and SEM (B) images of core—shell structure nanofibre membrane, and (c) Masson's trichrome staining of cranial defects in the at 4 and 8-weeks after implantation. Residual scaffolds are marked by a green asterisk, and newly formed bone is outlined by a yellow line. Bar represents 500 μm for all panels. Adapted from [58].
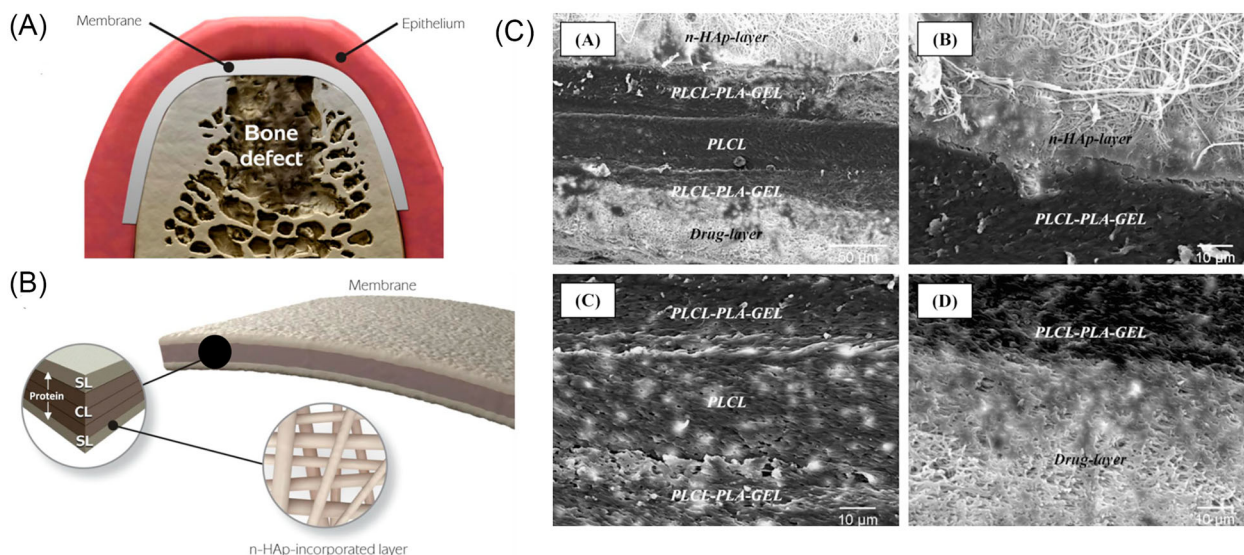
Figure 6. Schematic illustration of the spatially designed and functionally graded (FGM) periodontal membrane. (a) Membrane placed in a guided bone regeneration scenario and (b) details of the core-layer (CL) and the functional surface-layers (SL) interfacing bone (nano-hydroxyapatite, n-HAp) and epithelial (metronidazole, MET) tissues. Note the chemical composition step-wise grading from the CL to SLs, i.e. polymer content decreased, and protein content increased. (c) Cross-section SEM micrographs of the FGM processed via multilayering electrospinning. Adapted from [42].

GTR and GBR membranes face a complex environment where the soft tissue is more prone to be an open path for bacterial colonisation in case of dehiscence, while the hard tissue needs the proper cell source and regenerative stimuli without being disturbed by soft tissue invagination or bacterial infection. Research has therefore led to the development of graded structures that allow not only for tissue-specific compositions, but also to endow multifunctionality, such as infection control and regenerative cues to stimulate regeneration. Our group reported on the fabrication of a spatially designed and functionally graded membrane with unique therapeutic properties (Figure 6) [42]. The innovative membrane was designed and processed to display a core layer (CL) and two functional surface layers (SLs) to interface with hard and soft tissues. The CL was engineered by spinning a poly(DL-lactide-co-ε-caprolactone) (PLCL) layer surrounded by two composite layers consisting of a gelatin/polymer blend. Hydroxyapatite nanoparticles were incorporated to enhance bone formation on the SL facing the bone defect and metronidazole (MET) was added to inhibit bacterial colonisation on the SL facing the epithelial tissue. Worth noting, no delamination of the multilayered structure was observed upon mechanical loading, thus potentially assuring suitable surgical handling and physiologic loading *in vivo* [42]. In a similar study, a poly(L-lactide-co-d,l-lactide)-based functionally graded membrane was developed using platelet-derived growth factor as the SL facing the bone defect and MET facing the soft tissue [60]. Along with 28 days of sustained GF release, alveolar ridge regeneration was reported [60].

In sum, the development of GTR/GBR membranes by electrospinning holds significant translation potential, as it allows the use of a wide variety of polymers for fabrication of nanofibres and provides an ease of encapsulating additives such as drugs, antibacterial agents, and growth factors key in bone and periodontal tissue regeneration. Importantly, functionally graded and/or multilayered scaffold processing strategies, in addition to core–shell electrospinning approaches, can be leveraged to develop tissue-specific (hard *vs.* soft tissue) membranes with multifunctional properties.

Despite the impressive contribution made by electrospinning to the development of membranes and scaffolds for bone and periodontal regeneration, this technique presents intrinsic limitations. For example, electrospun fibres are generally closely packed in two-dimensional (2D) mat-like structures, which can adversely affect cell infiltration limiting tissue ingrowth and vascularisation. To support true physiological regeneration of the periodontal tissues, the scaffold must facilitate cell penetration and blood vessels formation to improve healing. Additionally, limited control while designing defect-specific scaffolds and the use of hazardous solvents to solubilise the polymer(s) of interest, have prompted the search to more suitable technologies with the potential to realise anatomically complex personalised scaffold geometries. Melt electrowriting (MEW), a relatively new additive manufacturing technology, provides a more biologically compatible alternative for processing nano/microfibrous scaffolds. The fibres can be precisely positioned to control the shape, porosity, fibre diameter and

mesh-width in three-dimensions [75,76]. This processing versatility is especially important for bone and periodontal tissue engineering and has been recently exploited to customise structural gradients or zonal tissue constructs [77,78].

Three-dimensional (3D) printing

3D printing has emerged as a unique manufacturing toolset within the fast-evolving field of regenerative medicine. This class of materials processing technologies allows the generation of patient- and defect-specific scaffolds and/or living constructs with finely tuned internal and external morphologies that approximate to the native tissue architectures. Not surprisingly, the utilisation of different biomaterial classes to engineer cell-free or cell-laden 3D scaffolds or implants has experienced a significant increase in recent years to fulfil the complexity and efficiency requirements for clinical translation [14,79]. A key advancement compared to more traditional processing methods of scaffold development is the intrinsic ability to place cells and/or biomolecules at predefined locations within the generated 3D scaffold microenvironment. Clinically speaking, recent advances in 3D printing technologies could, in the near future, eliminate the need for bone transplantation in large and geometrically complex CMF reconstructions, thus avoiding the creation of secondary bone defects.

3D printing comprises a wide array of fabrication technologies of which the most established are light-laser-, droplet-, and extrusion-assisted printing [27,80]. To date, extrusion-based printing has been the most employed method for bone and periodontal tissue applications, due to its versatility and affordability [81]. As the name indicates, extrusion printing involves the dispensing of molten polymers, bioceramic pastes, or hydrogels through an extrusion nozzle via pneumatic, piston-driven, or screw-driven force, resulting in the printing of continuous filaments to create predesigned architectures [33]. This technique can be used to print a wide range of porous and geometrically complex scaffolds with controlled mechanical and biological properties [12,13,28,33, 81].

The incorporation of biomolecules (e.g. growth factors) or therapeutic compounds within 3D printed scaffolds further provide additional means to help guide and ultimately improve the regenerative outcome [82–84]. Of note, coaxial and multimaterial dispensing systems have proven to be compatible with extrusion-based technologies [31,85,86]. One important advantage of this method relates to its ability to generate reproducible heterogeneous structures (e.g. shape, size, porosity, pore geometry, etc.) with multiple cell types at physiological densities carefully positioned at different locations on a complex scaffold/construct architecture [13,31,37]. Worth noting, the

method of printing live cells to create tissue-like structures that imitate native tissues is known as bioprinting. During bioprinting, a biomaterial solution in the form of a hydrogel or its precursor embedded with the desired cell type(s), termed the bioink, is utilised to create tissue-like structures in a layer-by-layer fashion. The aqueous 3D microenvironment provided by hydrogels simulates the natural ECM and then considered excellent candidates for the incorporation of cells [87]. However, given the high degree of freedom to use diverse biomaterials and cell types to engineer 3D constructs, in this section, we will discuss the most common cell-free and cell-laden extrusion-based printing techniques for craniofacial bone and periodontal regeneration. Extrusion-based printing can be classified into two main categories: thermal and non-thermal extrusion printing (Figure 7). Fused deposition modelling (FDM) is the major representative of polymer-based thermal extrusion; whereas melt electrowriting (MEW), which combines thermal extrusion and an applied electrical field, has been introduced to increase the resolution of the polymeric filaments down to the micron and sub-micron range. This technology has been deemed as a more refined version of the FDM method and has gained the spotlight in regenerative medicine due to its potential to engineer highly ordered fibrous scaffolds, capable of replicate extracellular microenvironment functions. Among the non-thermal extrusion-based 3D printing technologies, the pressure-assisted microsyringe is the most common approach and has been utilised to print bioceramic pastes and cell-laden hydrogel-based scaffolds (Table 2).

Thermal extrusion-based printing

Fused deposition modelling
Fused deposition modelling (FDM) was invented and patented by Scott Crump in the late 1980s [141]. The FDM method is based on the layer-by-layer printing of thermoplastic polymers. In this technique, the polymer of interest is heated above its melting point and due to a solid-semisolid state transition, is then extruded through a nozzle according to the predefined computer-aided-design (CAD) design [142]. After the first surface layer has been deposited, the nozzle rises or the platform descends one layer in the Z-axis direction, and the process is repeated until the designed geometry is completed. The polymer fuses to create a cohesive layer until solidifying at room temperature. FDM printers usually built 3D structures with a filament diameter ranging from 160–700 μm depending on the polymer and pattern of the structure [142]. The quality of the extruded filament can be modified by adjusting the printing speed, construct orientation, and layer thickness. This technique has several advantages, such as high printing speed and the potential to
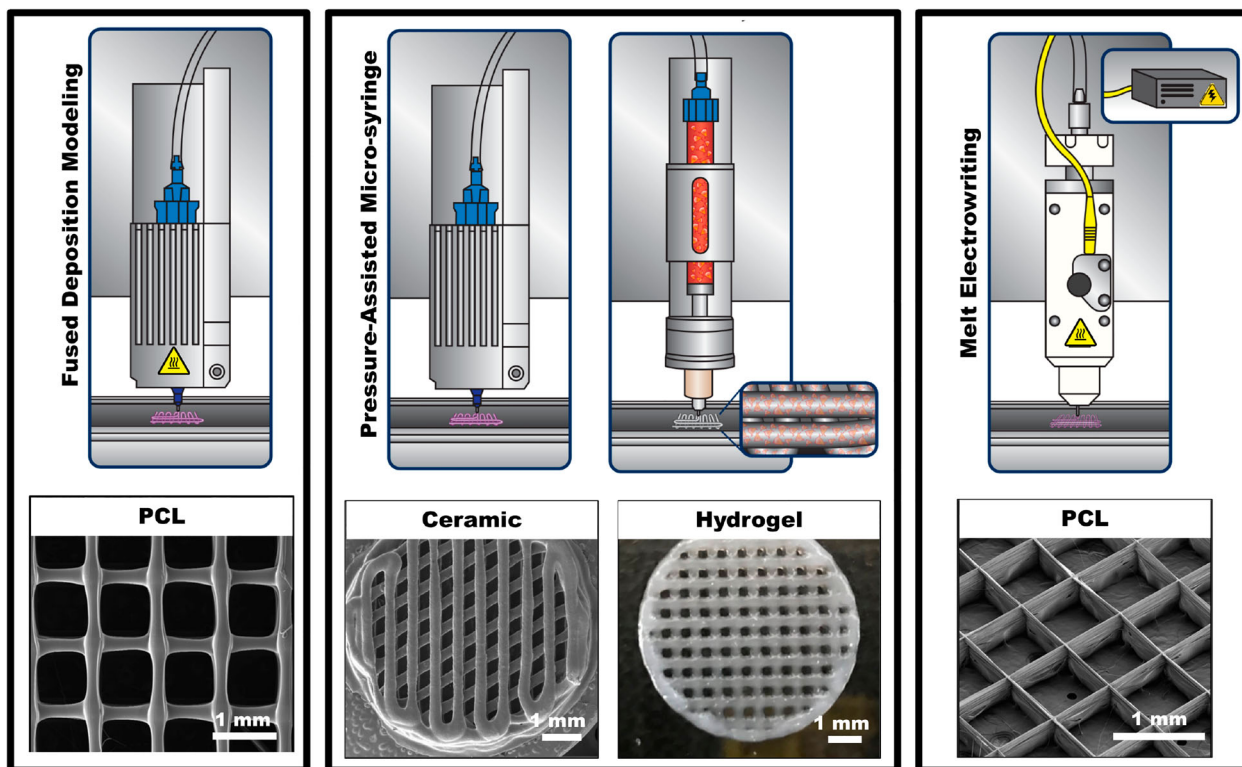
Figure 7. Schematic diagram of common extrusion-based methods with or without thermal extrusion for the printing of various biomaterials (polymer, ceramic, hydrogel) with high level of consistency.

print multiple materials simultaneously when working with a multi-nozzle printhead [11,143]. Furthermore, the FDM platform eliminates any possible toxicity induced by generally harsh organic solvents that are required for the solubilisation of polymers for electrospinning [144]. Nonetheless, limitations of this technique include low resolution and surface finish because material spreads out before it cools and hardens to the desired shape [145]. Yet, it is still possible to obtain resolutions similar to those achieved by other 3D printing techniques when utilising small diameter nozzles [145].

Biodegradable synthetic polymers, such as poly(ε-caprolactone) (PCL), poly(lactic acid) (PLA), and poly(lactic-co-glycolic acid) (PLGA) have been widely explored in FDM to generate scaffolds with tunable mechanical, chemical, and biological properties [88,89,145]. In a study by Shim et al. [88], PCL membranes with various porosities and pore sizes (up to 700 μm) were printed via thermal extrusion. After 14 days of *in vitro* culture, the membrane with 30% porosity showed higher osteogenic differentiation of pre-osteoblasts than those cultured on 50% and 70% porosities. Further, *in vivo* experiments were carried out to assess the regenerative efficacy of PCL membranes with different pore sizes upon implantation into rabbit calvaria defects. After 4 weeks, membranes with 30% porosity showed extensive bone formation, along with newly formed blood vessels [88]. In a different study, another interestingly described approach involved the utilisation of cold atmospheric plasma

to control nanoscale roughness of 3D printed PLA membranes aiming to enhance osteoblast and mesenchymal stem cells attachment and function [89].

Regrettably, although 3D printed polyester-based scaffolds with controlled porosity and surface modifications show good biomechanical and space maintenance properties for use in GTR/GBR applications, they present low bioactivity, and thus, lack therapeutic elements critical to the regenerative process. To amplify the regeneration capacity, bioceramics and/or growth factors (GFs) have been utilised to create composite scaffolds with improved bioactivity. Such a strategy was explored by Kim et al. [146], whereby a novel anatomically shaped rat incisor PCL/nHAp scaffold was fabricated via a layer-by-layer approach to deliver stromal-derived factor-1 and bone morphogenetic protein 7 (BMP-7). The scaffold was implanted into the extraction socket for orthotopic tooth regeneration and, after 9 weeks, scaffold within the socket showed new bone trabeculae-like structures with new periodontal ligament consisting of fibroblast-like cells and collagen-like structures immediately adjacent to new bone. The study highlighted that carefully selected GFs may recruit multiple cell lineages into the scaffold for regeneration of a putative periodontal ligament and newly formed alveolar bone [146]. Similar approaches where employed by others, where nHAp ranging from 10% to 40%, combined with 1,6-hexanediol L-phenylalanine-based poly(ester urea), were printed with 75% porosity and 300 μm pore size to enhance mechanical competence and impart

Table 2. Selected references on 3D (bio)printing strategies in craniofacial bone and periodontal tissue engineering.

Reference	Materials	Advantages/disadvantages	Most relevant findings
[88]	PCL	(+) production of resorbable membranes and tunable porosity	3D printed PCL with 30% porosity showed improved mechanical properties and osteogenic differentiation.
[82]	PCL/PLGA/Collagen	(+) short- or long-term release of BMP-2 can be achieved depending on the polymer used	Scaffold loaded with rhBMP-2 showed higher osteoinductivity compared to PCL/PLGA/gelatin loaded with rhBMP-2 or individual scaffold.
[89]	PLA	(–) requirement of the use of a post-modification method	CaP treatment of printed scaffold increased the roughness and hydrophilicity thereby positively impacting the proliferation of the osteoblasts.
[85]	PCL/PLGA/β-TCP	(+) similar levels of biocompatibility and bone regeneration as collagen membranes	3D printed membrane showed bone regeneration performance similar to that of collagen membranes during a GBR procedure performed in peri-implant defects.
[90]	PEU and HA	(+) capability of printing various types of polymers	3D printed HA-containing PEU composites promote higher bone regeneration compared to pure HA scaffold.
[91]	PLLA and β-TCP	(+) readily incorporation of bioactive tricalcium phosphate	*In vivo* bone formation driven by the PLLA + TCP30 scaffold with MG-63 cells was significantly greater than PLLA or TCP30 with MG63.
[92]	PCL/β-TCP/	(+) phlorotannin made the composites hydrophilic	Phlorotannin composites showed higher initial cell attachment and mineralisation than non-phlorotannin composite.
[93]	PCL-50 wt-% of 45s5 bioglass or strontium substitute bioactive glass	(+) biaxially rotating bioreactor cellular homogeneity throughout the scaffolds.	Release of ions (Sr, Zn, Mg, and Si) from scaffold accelerate angiogenesis and stimulate the osteogenic differentiation of mesenchymal stem cells (MSCs)
[84]	PCL-poloxamine	(+) tunable bioerosion rate and DEX release	Varying osteogenic activities from human mesenchymal stem cells cultured onto scaffolds composed of the various blends are demonstrated.
[94]	PLA	(–) difficulty in achieving biomimetic nano resolution	Angiogenesis and osteogenesis are successively induced by delivering dual growth factors with sequential release using PLA.
[83]	PCL/PLGA/β-TCP	(+) slow release of BMP-2	3D printed GBR membrane loaded rhBMP-2 exhibited significantly greater amount of new bone in the rabbit calvarial defect model compared to the membrane without rhBMP-2.
[95]	PCL	(+) combination of melt and solution electrospinning	The multiphasic construct with large and small pores electrospinning to develop biphasic scaffolds to supporting bone formation and cell sheets.
[96]	PCL, HA	(+) multiphasic scaffold to imitate native peridontium (–) ectopic peridontium formation	3D printed seamless scaffold with region-specific microstructure and spatial delivery of proteins resulted into putative dentin/cementum, PDL, and alveolar bone complex regeneration
[30]	PCL-PLGA	(+) printing complex structures by combination of FDM and electrospinning	Triphasic scaffold by combination of 3D printing (FDM) and electrospinning exhibited enhanced ALP activity and GAG amount.
[97]	PCL	(–) polymer of choice is limited because of the high melting point and biodegradability	MEW scaffold coated with calcium phosphate enhanced the osteogenic gene and protein expression of hOBs.
[98]	PLA-PEG_PLA and PLA	(+) tailoring scaffold architectures with high precision	5% BG did not affect the processing adversely.
[99]	PCL and HA	(+) precise and complex porous 3D fibrous structures & tunable porosity	Incorporation of HA in PCL increased the cell spreading and migration.
[100]	*P*-(Є-CL-co-AC)	(+) production of fibrous scaffolds with sinusoidal patterns and micron-sized diameter mimicking the ligament and tendons	MEW printed *P*-(Є-CL-co-AC) is cytocompatible and qualitatively mimicked the mechanical characteristics of tendon and ligament tissue.
[101]	Star PEG heparin hydrogel/ PCL	(+) multiphasic scaffold design in combination with different human cell type	Tissue-engineered periosteum constructs loaded with HUVECs and BMMSC enhance the vascularisation and retained the BM-MSCs in undifferentiated state *in vivo*.
[78]	PCL	(+) heterogenous porosity of scaffold increase cell attachment (–) study needs to be confirmed in an appropriate *in vivo* model	MEW scaffold with gradient pore size and fibre offset significantly improved the osteogenic potential.
[102]	PEOT, PBT, PCL	(+) designing structural porosity gradients	The construct with a discrete gradient in pore as a strategy to support differentiation supported the osteogenic differentiation of hMSCs.
[12]	PCL and GelMA	(+) reinforcing effect of meshes could be further (–) lack of detailed cross-linked kinetics of GelMA modified AMP.	Fibre-reinforced (PCL meshes processed via MEW) membranes in combination with therapeutic agent (s) embedded in GelMA offer a robust, highly tunable platform to amplify bone regeneration not only in periodontal defects, but also in other craniomaxillofacial sites.
[38]	GelMA, PCL	(+) convergent approach to combine extrusion-based printing of hydrogels and MEW	Mechanically stable constructs with the spatial distributions of different cell types without compromising cell viability and differentiation.

Table 2. Continued.

Reference	Materials	Advantages/disadvantages	Most relevant findings
[103]	Calcium silicate	(+) low-temperature rapid prototyping of C3S offers drug/GF incorporation during in printing process	Controllable nanotopography of printed structure into phosphate aqueous solution improve bone regeneration in vivo.
[104]	HA and Gelatin	(+) shape can be easily adjustable, in wet conditions, to that of the bone defect during surgery.	The osteogenic differentiation of MC3T3-E1 on silicon-doped HA scaffold was higher compared to HA only.
[105]	13--93 Bioactive glass/ alginate	(+) tunable pore size and porosity	With increase in BG/SA mass ratio, the pore size and porosity also increased. Furthermore, scaffolds exhibited in vitro apatite mineralisation and osteogenic differentiation of rBMSCs.
[29]	PCL	(+) Printed membrane-supported periodontal ligament fibrous cell sheets under both stationary and dynamic fluid conditions (−) standardised cell source for preparing the decellularised cell sheets.	Printed scaffolds improve the handling of the cell sheet during decellularisation protocols.
[106]	Sr-MBG	(+) Microfill perfusion assay to determine blood vessel. (−) in depth understanding of synergistic osteogenic/angiogenic effect of Sr and Si ions released.	Sr-ions from scaffolds create a better microenvironment activating the angiogenesis and osteogenesis pathway for the enhanced in vitro and in vivo bone formation.
[107]	βTCP-collagen	(+) heterophasic construct design	Scaffold allowed the proliferation of DPC and increased the differentiation towards osteoblasts.
[108]	Akermanite- βTCP	(+) repair of load-bearing bone defects.	Akermanite had better mechanical properties and a higher rate of new bone formation than the pure TCP scaffold.
[109]	Sodium alginate, Pluronic F-127, Bredigite bioceramic	(+) Better oxygen and nutrient delivery for cell activity	Enhanced vascularised bone formation due to synergistic effect of 3D printed hollow-pipe structure and release of bioactive ions.
[110]	Akermanite, Sodium alginate, Pluronic F-127	(+) scaffold developed with different raw materials including ceramics, metal and polymer.	Lotus root-like biomimetic materials significantly improved in vitro and in vivo osteogenesis and angiogenesis.
[111]	Calcium Phosphate	(+) fabrication of humidity-set scaffold	CPC containing VEGF maintains hMSC viability and bioactivity of HDMEC.
[112]	βTCP, Alginate and Gelatin	(+) Printable bioink at room temperature to load drugs/GF	Cell adhesion and ALP expression was enhanced by scaffold containing PLGA microspheres with VEGF.
[113]	Collagen, chitosan, HA	(+) tailored scaffold property for long-term controlled drug release and bone regeneration	The bone regeneration capacity of HA scaffold coated with collagen/chitosan microsphere with rhBMP-2 was higher than the HA scaffold coated with collagen or pure HA.
[114]	Mesoporous silica/calcium phosphate	(+) well-interconnected macropores and ordered mesopores	MS/CPC/rhBMP-2 scaffolds induced the osteogenic differentiation and vascularisation in vitro and in vivo.
[115]	β-TCP	(+) use of large translational animal model	Delivery of dipyridamole improved the osseoconduction in sheep calvarial defect model resulting in significant increase in bone formation.
[116]	Alginate, Pluronic F-127, bioceramic	(+) migration of cells in the inner part of the scaffolds due to high porosity and surface area	HSP demonstrated more new bone formation compared with a solid-struts-packed scaffold.
[117]	β-TCP, Wollastonite, Bredigite	(+) Scaffold stable in aqueous medium for a long period of time.	CSi-Mg10 scaffolds displayed improved flexural strength and higher osteogenic capability in rabbit mandibular defect.
[118]	β-TCP	(+) scaffold strut and porosity designed to elicit bone-healing behaviour.	3D printed beta-TCP induce new bridging bone formation in full-thickness mandibulectomy defects after 8 weeks without the use of osteogenic inducers.
[119]	PLGA-TCP	(+) Bone was able to remodel under physiological loading	Phyto-molecule icariin exhibited improved biodegradability, biocompatibility, and osteoinductivity both in vitro and in vivo.
[36]	Calcium phosphate, Alginate and Methylcellulose	(+) post-plotting regime, to prevent microcrack formation inside CPC strands	Biphasic scaffold showed migration of cells towards CPC from alg/mc after 7 days.
[120]	Alginate, Lutrol F-127, Poloxamer 407, Matrigel, Agrose, Methylcellulose	(+) two distinct cell populations printed within a single scaffold	No difference in cell proliferation and viability of 3D printed and unprinted hydrogel scaffolds.
[31]	α-TCP and type 1 collagen	(+) two step printing process to develop cell-loaded bioceramics scaffold.	3D printed scaffold showed improved physical properties, metabolic activity and mineralisation, compared with those of the controls.
[13]	AMP and synthetic peptide gel	(+) Fast degradation of AMP microparticles	AMP-modified constructs favoured in vitro and in vivo mineralisation without the use of a chemical inducer.
[121]	Collagen, β-TCP	(+) unique fibrillogenesis of collagen to produce a bioink laden with cell and bioceramics	hASC-laden composite structure (20 wt-% of β-TCP) demonstrated significant osteogenic gene expression compared to control cultured using an osteogenic media
[122]	GelMA,k-Carrageenan, Laponite	(+) NICE bioink produce fabricate patient specific, 3D implantable scaffold	bone tissue formation was a result of endochondral differentiation of hMSCs
[32]	PCL, Alginate	(+) MtoBS is a promising system for regeneration of heterogeneous tissue	Multi-Arm BioPrinter enabling dispensing of human chondrocytes and MG63 cells to biofabricate osteochondral tissue.

(Continued)

Table 2. Continued.

| Reference	Materials	Advantages/disadvantages	Most relevant findings
[123]	Agrose hydrogel	(+) computationally designed spatial patterns of cells	3D printed constructs with specific spatial pattern and varying cell densities improves cell viability
[37]	PCL, Alginate, Collagen, HA	cytocompatible multi-layered construct formed by stacking different types of printable extracellular matrix (ECM) bioink	3D printing of construct with different types of ECM hydrogels encapsulated stem cells allowed the differentiation towards chondrogenic and osteogenic lineages
[124]	Alginate, chitosan	The coating improved the retention and release efficacy of drug	The coating of 3D printed alginate construct with chitosan improved cell proliferation and result into elongated cells.
[125]	β-TCP	(+) Scaffold preserved the cranial suture patency.	Large scaffold pore (500 μm) coated in 1000 μM dipyridamole yielded the most bone growth and faster degradation within the defect.
[14]	PCL	(+) first clinical case of 3D printed scaffold for periodontal regeneration. (−) Slow scaffold resorption, at 13 months, the scaffold became exposed	The implanted 3D scaffold showed n signs of chronic inflammation or dehiscence upto 12 months.
[126]	PCL	(+) scaffolds combined hierarchical mesoscale and microscale features can align cells *in vivo*.	Combination of gene therapy and topographical guidance cues showed osseous tissue formation and oriented collagen fibres for treatment of periodontal osseous defects.
[77]	GelMA, PCL	(+) convergence of MEW and bioprinting, for fabrication of flat to anatomical relevant structures.	MEW process allowed the fabrication of a complete condyle-shaped biological construct.
[127]	PCL, MBG-58S	(+) use of clinically relevant post-menopausal mode; for bone regeneration	MBG-PCL scaffold promoted new bone formation at both the peripheral and the inner parts of the scaffolds with thick trabeculae and a high vascularisation degree.
[128]	PCL, Mesorporous calcium silicate and bioactive glass	(+) two different scaffolds with highly properties to avoid the interference of the comparing osteogenic potential	MBG/PCL scaffolds exhibited better bioactivty than MCS/PCL scaffolds for bone regeneration.
[129]	Magnesium phosphate	(+) DAHP solution eliminate the conventional sintering process to extend the usefulness of loading drug	MgP scaffold showed good pore structural conditions, mechanical property and cell affinity.
[130]	α-TCP	(+) fabrication of thermally instable and degradable matrices of secondary calcium phosphates	binder enabled the fabrication of custom made brushite/TCP implants with well-defined architecture and the ability of being resorbed in vivo binder enabled the fabrication of custom made brushite/TCP implants with well-defined architecture and the ability of being resorbed in vivo The printed sample strength increase after treatment of phosphoric acid give rise to brushite with minor phases of unreacted TCP.
[131]	TCP, DCPA	(+) complete conversion of all components involved in the production process (raw powder and binder solution) to a cement matrix minimising risk of harmful residues	Scaffolds was printed with >96.5% of dimensional accuracy. Cell proliferation was higher on biphasic calcium phosphate when compared to HA.
[132]	CaP, PCL, GelMA	(+) Multi-material, multi-scale 3D printing approach (hydrogel-thermoplastic-bioceramic composite)	multi-scale composite osteochondral plugs results in the formation of cartilage-like matrix *in vitro* with 3.7-fold increase in strength of the interconnection at the bone-cartilage interface.
[133]	Calcium silicate, β-TCP	(+) engineering of pro-angiogenic microenvironment *in vitro*	Co-culture of HUVECs and hBMSCs on porous 5% CS/β-TCP accelerates vascularisation and osteogenesis in ectopic bone formation model.
[134]	GelMA	(+) hollow, stackable miniaturised microcage modules, resembling the features of toy interlocking building blocks	3D printed microcages loaded with microgels supplemented with growth factors enhanced cell invasion into the core of assembled constructs in a controllable manner, thus accelerating the process of new tissue formation and healing.
[135]	β-TCP	(+) scaffolds do not cause premature closure of sutures and preserve normal craniofacial growth	Regeneration of vascularised bone with mechanical characteristics comparable to native bone.
[136]	PCL	(+) high adaptability to the created defect geometry	The ligament cells displayed highly predictable and controllable orientations along microgroove patterns on 3D biopolymeric scaffolds.
[137]	β-TCP	(+) Dipyridamole as a viable cost-effective osteogenic agent	Resorbable, β-TCP scaffolds treated with DIPY increased bone regeneration qualitatively and quantitatively.
[138]	Akermanite	(+) Development of Haversian bone–mimicking scaffolds (−) multicellular synergistic including bone-resident cells such as osteoblasts, osteoclasts, and macrophages need to be explored	The scaffold showed the potential for multicellular delivery by inducing osteogenic, angiogenic, and neurogenic differentiation *in vitro* and accelerated the ingrowth of blood vessels and new bone formation *in vivo*.
[139]	TCP and anhydrocus dicalcium phosphate	(+) discrete deposition of pharmaceutical agents on bioceramics scaffold using multijet 3D printing	rhBMP-2 and vancomycin by loading the drug within the 3D printed scaffold.
[140]	PCL	(+) deferoxamine loaded PCL showed mechanical property similar to cancellous bone	The deferoxamine-printed scaffold had no effect on cell attachment or proliferation, but it significantly increased vascularisation, which was accompanied by increased bone growth.

bioactivity [90]. The composite scaffold with 40% nHAp led to accelerated osteogenic differentiation; however, there was a decrease in the scaffold's compressive modulus when the temperature increased to a physiological value [90]. Several other investigations have followed the same approach by blending nHAp to increase osteogenesis of polymer-based 3D printed biodegradable scaffolds [147,148].

β-tricalcium phosphate (β-TCP) is another important bioceramic due to its intrinsic osteoconductivity and faster degradation rate when compared to traditional HAp. Distinct amounts (10–30%) of TCP were mixed with poly(lactic acid) to obtain scaffolds with an orthogonal design and 100 μm pore size. After 12 weeks *in vivo*, the degradation of the scaffolds matched that of new bone formation (Figure 8(a,b)) [91]. A similar strategy was used to print β-TCP/PCL scaffolds. The scaffold with 30% TCP, under mechanical stimulation, led to the upregulation of bone-related genes. From a mechanical standpoint, the compressive modulus of the fabricated scaffold was comparable to human trabecular bone [92]. Meanwhile, synthetic biodegradable polymers have also been modified with bioactive glasses (BGs) due to their ability to form an intermediate apatite layer and stimulate osteogenic differentiation [105,127]. In a recent study, 3D printed PCL-based scaffolds modified with 50% 45S5 BG or Sr-substituted BG were able to stimulate osteogenic differentiation of bone marrow stromal cells without additional chemical inducers [93].

The incorporation of therapeutic agents has also been explored in the development of 3D printed scaffolds for vascularised bone regeneration [82,83].

As an example, dexamethasone-loaded 3D printed scaffolds made of PCL and poloxamine demonstrated to be a viable option to locally deliver biomolecules to induce osteogenic differentiation of resident mesenchymal stem cells (MSCs) (Figure 8(c,d)) [84]. In another study, 3D printed PLA scaffolds with defined pore size (200 μm) were coated by a layer-by-layer nanocoating technique for sequential release of angiogenic and osteogenic GFs to generate vascularised bone constructs. The co-culture of human umbilical vein endothelial cells and bone marrow-derived MSCs on 3D printed nanocoated scaffold exhibited excellent bone forming potential with well-developed microvascular networks [94]. A unique approach was employed by Shim et al. [83] in the fabrication of PCL/PLGA/β-TCP 3D printed membranes with controlled pore size (250 μm), following which a collagen/rhBMP-2 mixture was dispensed into the membrane's empty pores. The collagen/rhBMP-2 solution was physically gelled at 37°C prior to implantation. Upon euthanasia, the animals receiving the collagen/rhBMP-2 filled constructs showed 70% of total new bone formation compared to 40% in the case of unfilled (control) scaffolds [83].

Although the aforementioned scaffold strategies are promising to regenerate vascularised craniofacial bone, they fall short of their ability to facilitate the coordinated regeneration of multiple periodontal tissues, which includes not only alveolar bone, but also cementum and periodontal ligament (PDL). In the complex architecture of the periodontium, the regeneration of bone is correlated with the neoformation of cementum and PDL. Therefore, to allow multi-tissue periodontal regeneration, multiphasic scaffolds with
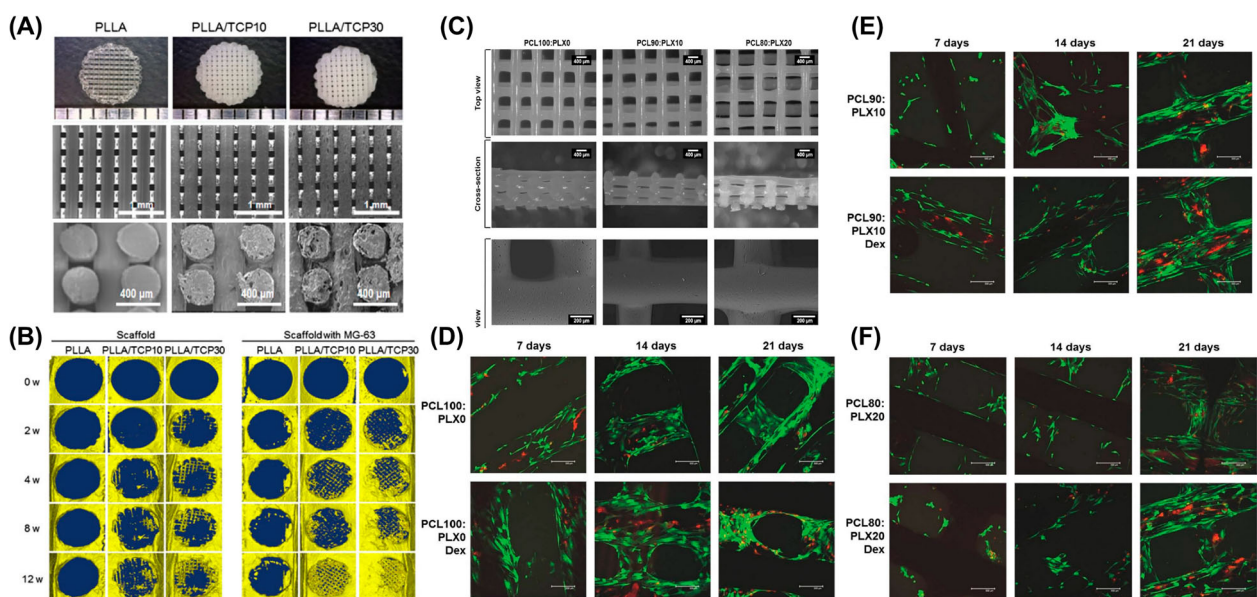
Figure 8. (a) Images of the prepared scaffold (1) photograph, (2) micrograph, and (3) scanning electron microscopy, (b) Micro-CT images from rats that received the scaffold at 0–12 weeks after implantation. Adapted from [91]. (c) Imaging of scaffold's architecture and surface morphology by stereomicroscopy. (d-f) Confocal imaging of live (calcein, green) and dead (propidium iodide, red) human mesenchymal stem cells cultured onto the scaffolds. Adapted from [84].

structural arrangement, and unique architectural and chemical characteristics, should be devised to mimic the periodontium's highly organised zonal structure. To this end, Vaquette et al. [149] developed biphasic 3D printed scaffolds made of PCL and 20% β-TCP with 70% porosity and 100% interconnectivity to form the bone zone. The periodontal ligament (PDL) zone was created by electrospinning of a PCL solution to support and deliver mature PDL cell sheets. The aforementioned biphasic scaffold was coupled with a dentine slice and implanted in an athymic subcutaneous rat model. The investigators observed that 67% of the test group with PDL cell sheets showed new cementum-like tissue on the dentin surface, compared to 17% for the group without PDLC sheets [149]. Taken together, the regenerative outcomes achieved with biphasic scaffolds have opened up new horizons in terms of how the meticulous design of bone and PDL zones are critical in the process of periodontal tissue regeneration. Nonetheless, cementogenesis, i.e. the neoformation of cementum remains a challenging issue, as it relies on endogenous cells to facilitate cementum deposition on the root dentin surface. In this way, the consideration and implementation of a third tissue-specific zone has shown to play a key role in enabling the regeneration of cementum and supporting the controlled alignment of PDL fibres. In this context, triphasic PCL/HAp composite scaffolds have been designed with a tissue-specific zonal arrangement presenting distinct microchannel diameter (100, 600, and 300 μm for cementum, PDL, and bone zones, respectively), thus allowing the creation a hierarchical tissue-specific zonal scaffold. Importantly, PLGA microspheres loaded with regenerative cues, such as amelogenin (cementum), connective tissue growth factor (PDL), and BMP-2 (bone), were introduced into each particular zone to enhance tissue-specific cell differentiation. *In vitro* studies were performed by seeding alveolar bone, periodontal ligament, and dental pulp stem cells along with zone-specific GFs coupling, led to the formation of new bone and cementum-like tissue. Scaffolds seeded with DPSCs generated aligned PDL-like collagens adjacent to newer bone and cementum, which shows that the successful spatio-temporal delivery of distinct proteins can differentiate individual cells into multitissue periodontal complex *in vivo* [96]. In another example, Criscenti et al. [30] combined 3D printed PCL scaffolds and electrospun PLGA nanofibres to obtain triphasic scaffolds to mimic the zonal microenvironment of the bone-to-ligament interface. First, PCL scaffold, designed with a 700 μm fibre diameter and 150 μm fibre spacing, was printed to serve as a bone zone and then, two-thirds of this scaffold was coated with electrospun aligned PLGA nanofibres to mimic the ligament for the regeneration of bone-ligament

interface. 3D printed, hybrid, and electrospun regions were the three regions in the aforementioned triphasic scaffold. This scaffold mimicked the gradient structure of bone-ligament. MSCs were distributed homogenously, not only at the interfaces, but also throughout the entire scaffold. Glycosaminoglycan (GAG) analysis showed higher GAG content for the triphasic scaffold than the controls, indicating improved ligamentogenesis. The results clearly indicated that hMSCs behaviour is dependent on the scaffold fabrication method. Briefly, a combination of two techniques (3D printing and electrospinning) provides advantages for interface tissue engineering by mimicking the bone-ligament interface in terms of mechanical, structural, and biological properties [30].

Melt electrowriting

Apart from the traditional thermal extrusion methods of polymer printing, a technique named melt electrowriting (MEW), that combines the principles of thermal polymer extrusion and electrospinning, was established to print filaments, which are at least 10 orders of magnitude thinner than conventional FDM. Notably, MEW allows printing highly ordered porous scaffolds/constructs with filaments ranging from ∼ 2–3 μm to 30 μm [12,75,142], with recent research demonstrating the possibility to obtain nano-sized polymeric filaments when using acupuncture needles as the spinneret [76].

A wide array of degradable polymers has been used to generate MEW scaffolds, with PCL being the most investigated one. In order to achieve higher resolution and overall control of the construct's architecture, key processing parameters have been identified, such as flow rate of the polymer melt, speed of the collector, spinneret diameter, distance from the needle tip to collector, and applied electric voltage. Optimisation of the aforementioned variables allows the formation of a stable, continuously drawn polymer melt directly from the spinneret over the translating collector to realise highly ordered 3D architectures [76,150]. A strategic driver for the latest advances associated with MEW is the rapidly evolving field of regenerative engineering, including, hard and soft tissue regeneration. In one of the seminal studies, PCL scaffolds were prepared using MEW and then modified with a CaP coating to increase cell attachment and osteoinductive properties [97]. Human osteoblasts (HOBs) seeded on these scaffolds showed upregulation of an osteogenic-related gene (osteocalcin); whereas, upregulation of fibronectin and vitronectin was reported for PCL scaffolds etched with sodium hydroxide [97]. Similarly, melt electrowritten poly(lactide-block-ethylene glycol-block-lactide) (PLA-PEG-PLA) scaffolds containing 45S5 BG were recently reported as another viable alternative to endow bioactive

properties to polymeric MEW scaffolds for bone tissue engineering applications [98].

Porosity is one of the main factors promoting cell migration, proliferation, and most importantly vascularisation of engineered tissues. As previously described, the optimum pore size for bone regeneration is in the range of 150–300 μm. In a study by Abdalla Abdal-hay et al. [99], composite scaffolds composed of PCL and HAp nanoparticles (3–7%) were produced via MEW to mimic the morphological and structural properties of bone. As the amount of HAp increased, cell spreading and migration also improved. Incorporation of HAp caused scaffold degradation to be faster than in alkaline conditions, which is the pH during the healing of wounds. Scaffolds with large (190 μm) interconnected pores with a high porosity (96–97%), and the presence of HAp was observed to facilitate cell infiltration and growth [99]. Alternatively, in a study by Hochleitner et al. [100], photocrosslinkable poly(L-lactide-co-ε-caprolactone-co-acryloyl carbonate) and poly(ε-caprolactone-co-acryloyl carbonate) were used to produce a sinusoidal pattern to mimic the ultrastructural and mechanical properties of native ligament and tendon tissues. The slightly sinusoidal engineered fibres were crimped enough to approximate to the non-linear stress–strain response of native tendon and ligament. This sinusoidal scaffold exhibited an improvement in cyclic fatigue testing as compared to the scaffolds composed of straight fibres thanks to their geometry. As a result, MEW technology can generate scaffolds that mimic the biomechanical behaviour of crimped collagen type I found in natural tendon and ligament tissues [100].

As previously highlighted, the engineering of zonal, tissue-specific scaffolds in terms of both composition and architecture has been deemed crucial to the coordinated growth and regeneration of both soft and hard periodontal tissues. In a study by Vaquette et al. [95], matured cell sheets, including periodontal ligament cells (PDLC), gingival cells and bone marrow-derived MSCs delivery system was developed using a biphasic scaffold fabricated by a combination of solution electrospinning and melt electrowriting (MEW). The bone zone with macroscopic pores was obtained via MEW, whereas the periodontal region was created by a flexible electrospun mesh to support cell sheet delivery. The scaffolds were placed *in vivo* in artificially created periodontal defects in a sheep model and revealed excellent tissue integration between bone and PDL. Importantly, a greater bone fill was seen in the PDLC group after 10 weeks. Histological analysis demonstrated the formation of new bone, cementum, and obliquely inserted PDL fibres [95]. Similarly, tubular PCL scaffolds were obtained by using MEW as a tissue-engineered periosteum construct. Periosteum,

which provides blood supply to the cortical bone and osteogenic niche, is of great importance for bone homeostasis and regeneration. A new concept was introduced by using MEW 3D printed tubular scaffolds and different cell types for periosteal regeneration *in vivo*. Star-shaped poly(ethylene glycol)-heparin hydrogel incorporated with HUVECs and PCL tubular scaffolds seeded with BMSCs were combined to mimic periosteum's multiphasic structure. The scaffolds were placed around the femur in contact with bone, aiming at recapitulating both the vascular and osteogenic niches. The results demonstrated that human bone marrow-derived MSCs maintained its undifferentiated phenotype over 30 days of *in vivo* culture, which was mainly attributed to the properties of the hydrogel; whereas, HUVECs developed into mature vessels with increased vascularisation compared to the cell-free approach [101].

The generation of scaffolds with a porous and porosity gradient can lead to 3D architectures that resemble the structure of native bone tissue with gradually increasing pore size from one layer to the next mimicking the changes in mineral density from cortical to cancellous bone [102]. Abbasi et al. [151] developed highly ordered MEW constructs with different pore sizes (250, 500, and 750 μm), two offset constructs of 30% and 50% layout, and a gradient construct of 250–500–750 μm (Figure 9(a)). The constructs were modified with CaP to boost osteogenic differentiation. The findings indicated that gradient constructs led to more pronounced ALP activity, while mineralised matrix deposition (Figure 9(b)) was higher in the 50% offset constructs. The expression of osteogenic genes was also upregulated in offset and gradient constructs [102].

Another interesting strategy examined the reinforcing effect of MEW PCL meshes upon integration with gelatin methacryloyl (GelMA) hydrogels [12,152,153]. As an example, our research group recently reported on a multifunctional membrane for guided bone regeneration (Figure 9(c,d)) with predictable mechanical competence and therapeutic features using a highly porous MEW PCL fibre-reinforced hydrogel laden with amorphous magnesium phosphate (AMP). The incorporation of AMP and MEW fibres into the hydrogel provided tunable mechanical strength and enhanced the osteogenic potential. The results showed that the presence of MEW PCL mesh retards the degradation and successfully prevent soft tissue invasion into the osseous defect (Figure 9(e)). It was concluded that the membrane acted as a bioactive barrier as the presence of AMP led to improved bone formation [12]. Although it was demonstrated that such composite scaffolds have improved mechanical and biological properties, the preparation of these constructs involved a two-
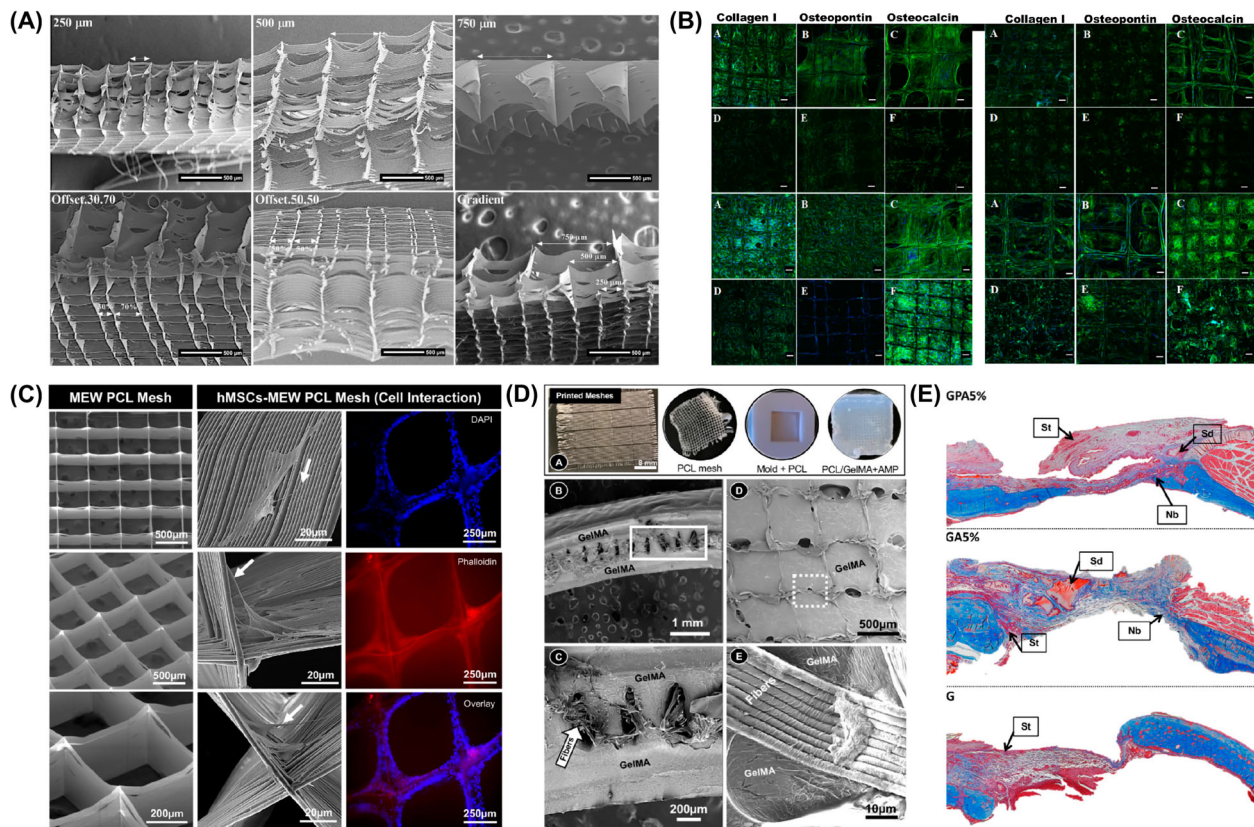
Figure 9. (a) SEM images of the porous MEW scaffold structures. (b) Immunocytochemistry analysis of osteogenitor markers (collagen I, osteopontin and osteocalcin) for human osteoblast cells cultured in (A, B, C) Osteogenic medium (D, E, F) Basal medium after 14 and 30 days. Adapted from [78]. (c) SEM and confocal micrographs of MEW PCL mesh and its interaction with hMSCs after 3 days. (d) Macrophotographs (A) detailing the steps involved in the fabrication of highly porous MEW PCL meshes with well-controlled 3D architecture and infusion with GelMA + AMP using a custom-made mould. (B-E) Representative cross-section SEM micrograph of the GelMA-PCL (GP) membrane showing the hydrogel phase uniformly infiltrated into the pores of the polymer mesh. (e) Masson's trichrome stained sections of implanted membrane showing the remnants of the GelMA surrounded by newly generating ossifying bone after 8 weeks in the bioactive hydrogel infused in the PCL mesh and bioactive hydrogel group, indicating slower degradation of GelMA in presence of AMP and PCL mesh. Adapted from [12].

step fabrication procedure, i.e. the generation of the reinforcing fibrous mesh followed by infusion of the hydrogel, which limited the freedom of designing microfibrous architectures, and the use of multiple materials and cell types in a controlled fashion. One important development in the evolution of the manufacturing of fibre reinforced cell-laden hydrogels is the potential to combine both hydrogel extrusion and MEW processes into a single biofabrication platform [38,40].

Non-thermal extrusion-based printing

The major limitation of thermal extrusion methods is the use of high temperatures, which may ultimately lead to denaturation of proteins and biochemical factors [33,154]. To solve this issue, extrusion-driven 3D printing of solutions and/or pastes (e.g. bioceramics), without material melting, has been proposed. Pressure-assisted microsyringe (PAM) uses a pneumatic-driven system to deposit, at room temperature, cell-free or cell-laden biomaterials on a substrate avoiding the denaturation of

temperature-sensitive biomolecules and/or cell death [155]. In this method, a semi-solid formulation with the necessary printing properties is used as the starting material to generate physically and mechanically stable 3D constructs. Therefore, the rheological characteristics of the biomaterial is an important property that affects the printing process and quality, and depends on the quantity and type of additives used to obtain the semi-solid formulation. A pressurised valve-free or valve-based air piston is usually the dispensing mechanism. Notably, the improved precision of the latter has motivated its widespread use [81,156]. Nonetheless, non-thermal extrusion-based 3D printing approach has been employed in the generation of bioceramics, hydrogels, and cell-laden scaffolds at low or physiological temperatures [13,157,158]. Next, we provide an overview of the most current work pertaining to non-thermal extrusion 3D printing opportunities for the fabrication of cell-free and cell-laden scaffolds with controlled geometry, architecture, and biological features for applications in craniofacial bone and periodontal regeneration.

Cell-free scaffolds

Bioceramics refer to a class of ceramic materials made up of inorganic crystalline oxide materials that are intrinsically biocompatible and can be processed compositionally and structurally to mimic native bone [159]. It is well-established that bioceramic scaffolds (e.g. hydroxyapatite [HAp] and beta-tricalcium phosphate [β-TCP]) have stimulating effects on stem cell proliferation and differentiation. Moreover, their tunable degradation permits them to be processed to provide structural support and guide bone regeneration [36,128].

Hydroxyapatite is the major inorganic component of bone and is responsible for its mechanical strength and, together with other CaP-based bioceramics, have been the most widely employed in bone tissue engineering [157]. Depending on their chemical composition, bioceramics can be inert or bioactive (i.e. ability to form hydroxyl apatite mineral on its surface both *in vitro* and *in vivo*). Over the last decades, bioceramics have been extensively utilised to formulate pastes and cements that can be injected into complex osseous defects that are challenging to realise with traditional bone grafting [103,110,117,118,160]. However, such complex bone defects can hardly be treated by pasty bone materials, but require the implantation of pre-formed scaffolds with complex and customised geometries. Thus, 3D printing has been deemed as a promising technology to fabricate patient-specific bone grafts from bioceramics [34,35]. Indeed, previous works have demonstrated the ability to manufacture, via 3D printing, customised bioceramic scaffolds [129–131,161] and also suggested the potential to incorporate additional bioactive additives [35,139].

In a study employing HAp and tricalcium silicate, a self-setting tricalcium silicate scaffold was fabricated with an up-and-down staggered structure using mechanical extrusion to facilitate subsequent cell seeding. The nHAp structure was created by immersing the printed structure in a predetermined phosphate aqueous solution at 37°C for 3 days. The presence of HAp on 3D printed tricalcium silicate scaffolds showed higher ability to induce osteogenic differentiation and bone formation *in vitro* and *in vivo*, respectively, compared to the pure 3D printed tricalcium silicate scaffold [103]. Research conducted by Martinez et al. [104] reported 3D printed scaffold of gelatin with Si doped HA microparticles using a pneumatic-driven extrusion method. The scaffolds exhibited compression strength close to that of trabecular bone. Mouse calvaria pre-osteoblasts seeded on these hybrid scaffolds upregulated the expression of osteogenic genes, such as runt-related transcription factor 2 and osteocalcin when compared with gelatin-free scaffolds [104]. Similarly, 3D printed composite scaffolds consisting of 13-93 BG and sodium alginate improved rat MSCs attachment and osteogenic differentiation [105]. Further, the release of bioactive ions from the scaffold contributed to apatite mineralisation *in vitro* [105]. In another study employing BGs, osteoinductive and angiogenic properties were enhanced by printing Sr-incorporated mesoporous BG [106]. Sr-doped BG scaffolds implanted into critical size defects in rat calvaria led to superior bone formation compared to BG scaffolds lacking strontium (Sr) doping. Microcomputed tomography showed improved vascularisation for the Sr-doped scaffolds, compared to non-doped scaffolds *in vivo* [106].

Beta-tricalcium phosphate (β-TCP) scaffolds were printed in a layer-by-layer fashion, with deliberate geometric design (250 μm struts and 330 μm pore) and evaluated in a clinically relevant translational *in vivo* model [118]. After 8 weeks of scaffold implantation in critically sized full-thickness (i.e. rabbit mandible), improved bone formation was observed in the absence of an osteogenic agent, and there was no significant difference in the baseline bone area occupancy between an unoperated mandible section (55.8 ± 4.4%) and new bone (54.3 ± 11.7%) [118]. To achieve improved osteogenic action, a multiphasic construct consisted of a 3D printed β-TCP scaffold with an interconnected porosity similar to that of bone was infused with a collagen matrix to mimic bone's extracellular matrix (ECM) to support the adhesion and osteogenic differentiation of dental pulp stem cells (DPSCs). After 21 days of *in vitro* culture, a marked increase in ALP activity of DPSCs was seen when compared to 3D printed β-TCP scaffolds devoid of collagen [107].

It is well-established that successful bone reconstruction in load-bearing areas requires a mechanically competent and bioactive scaffold. In this context, the addition of akermanite ($Ca_2Mg(Si_2O_7)$) to β-TCP led to the fabrication of a 3D printed scaffold with improved mechanical and regenerative (bone formation) properties than pure β-TCP control scaffolds [108]. Along with controlled mechanical and degradation properties, scaffolds' macrostructure also plays a role in bone regeneration [162,163]. Hollow strut-packed bioceramic-based scaffolds printed using a modified coaxial strategy with defined macropores and multi-oriented hollow channels led to greater bone formation compared to solid struts-packed scaffold [116]. Meanwhile, in another study, a core–shell printed structure of 1000 and 500 μm in diameter, respectively was realised to obtain scaffolds with a hollow pipe-stacked bioceramic structure (bredigite, $Ca_7Mg(SiO_4)_4$). The implantation of the uniquely designed (i.e. hollow pipe) scaffold in a radial segmental defect led to the early formation of new blood vessels and bone regeneration and remodelling within the bone defect [109]. A similar approach reported improved *in vitro* cell functions and *in vivo*
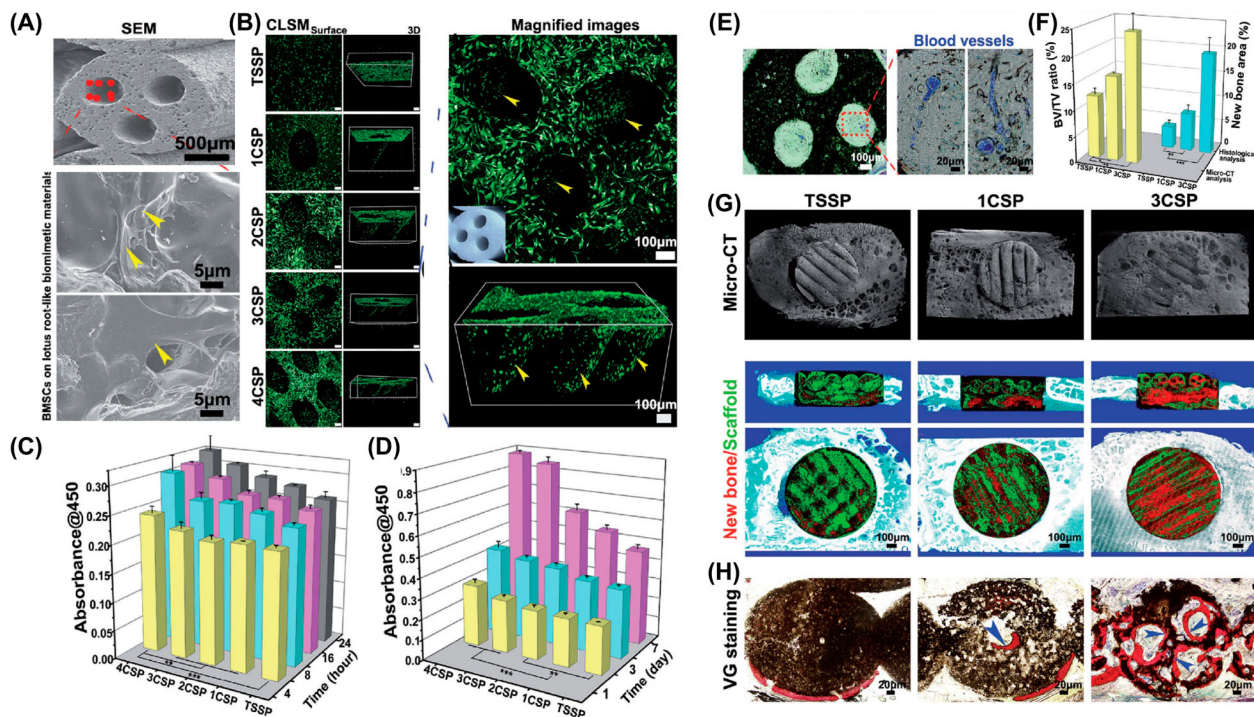
Figure 10. (a-b) SEM and confocal images for the morphology and cytoskeleton of BMSC cultured in TSSP, 1CSP, 2CSP, 3CSP, and 4CSP-AKT bioceramic scaffolds for 3 days. (c-d) The adhesion and proliferation of BMSC at different incubation time showing enhanced adherence and proliferation of cells with increase in channel numbers in the biomimetic scaffolds. (e) Fluorescence image of histological sections of biomimetic scaffolds stained with DAPI optical microscope image of 3CSP biomimetic scaffolds with blood vessels perfused by microfill. (f-g) Typical 3D reconstruction micro-CT images of the edges between materials and rabbit calvarial defects and analysis of the volume ratio of the newly formed bone to the defect regions (BV/TV). (h) The undecalcified histological sections stained with Van Gieson's picrofuchsin, newly formed bone tissues (in red) can be well observed (blue arrows point to the new bone). Adapted from [110].

angiogenesis for a lotus root-like scaffold with internal microfeatures (e.g. pores and microchannels) (Figure 10(a,b)). The proposed structure is beneficial for transferring oxygen, nutrition, and cell migration into the inner portion of the scaffold. After 12 weeks of implantation, the lotus root-like scaffolds led to greater angiogenic and osteogenic activity compared to conventional 3D printed scaffolds (Figure 10(c–h)) [110]. These studies have shown that macrostructures, mechanical strength, and ions' release positively affect cell penetration and proliferation, thus supporting osteogenesis and improved vascularisation. In addition, magnesium-based materials have recently received particular interest, due to their ability to chemically degrade *in vivo* and their high potential to promote bone regeneration. A striking example recently introduced by Golafshan and colleagues (2020), demonstrated the non-thermal extrusion printing of magnesium (Mg)-based 3D scaffolds (Figure 11(a,b)) with compressive strength and toughness similar to native bone, that led to mineralised tissue *in vitro* bone formation without the need of supplementation with osteoinducing components. In a 6-month *in vivo* validation in an equine model, the authors confirmed the osteopromotive potential and easy surgical handling of the novel Mg-based scaffolds (Figure 11(c,d)) [35].

Recently, various attempts have been made to enhance the healing of bone and periodontal tissues by the utilisation of growth factors to directly influence tissue morphogenesis [82–84]. Hence, the appropriate release of therapeutics from 3D printed scaffolds can provide key biochemical cues to boost tissue regeneration. Currently available 3D printing technologies have been able to generate geometrically complex scaffolds loaded with a wide variety of antimicrobial drugs and growth factors. In fact, the tunable porous structure of ceramics is suitable to the loading and release of biomolecules, such as proteins, polypeptides, or amino acids [164,165]. Akkineni et al. demonstrated the feasibility of printing, via pneumatic extrusion, CaP cement composite scaffolds premixed with chitosan/dextran sulphate microparticles for localised delivery of vascular endothelial growth factor (VEGF) [111]. Scaffolds loaded with VEGF demonstrated higher cell viability compared to control (VEGF-free) scaffolds and higher ALP activity of MSCs cultured on the scaffolds for up to 21 days [111]. Similarly, 3D printed β-TCP/gelatin/alginate composite scaffolds encapsulated with VEGF-releasing poly(lactic-co-glycolic acid) (PLGA) microspheres showed improved cell proliferation and attachment of HUVECs and osteoblasts when compared to control scaffolds [112]. Of note, VEGF-laden scaffolds promoted significantly greater
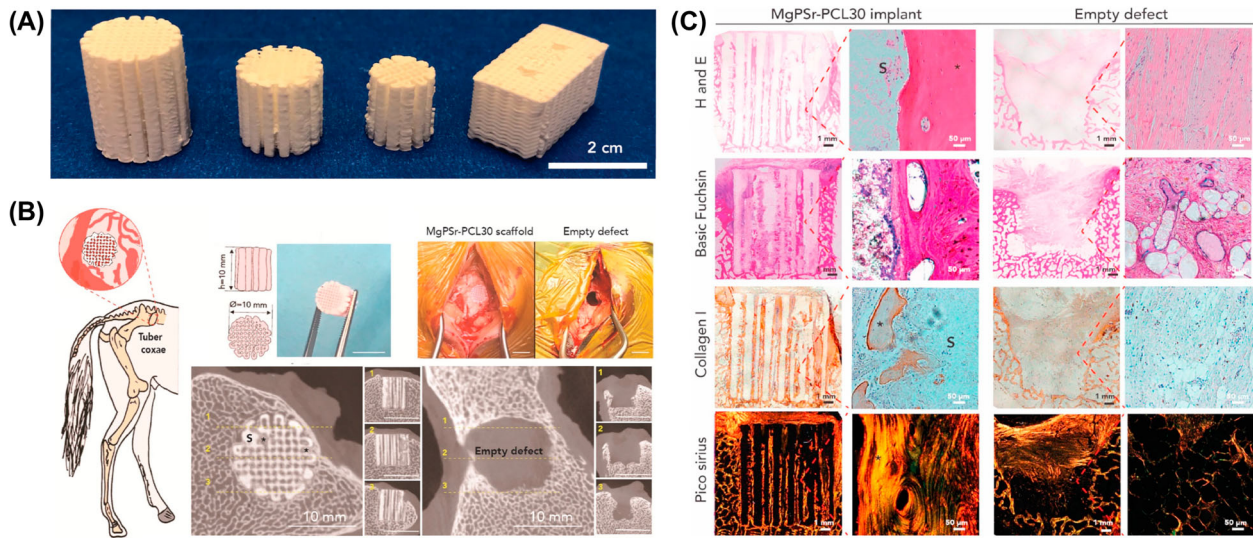
Figure 11. (a) Designed and printed scaffolds with various shapes of MgPSr-PCL30. (b) Schematic representation of the implantation of cylindrical constructs in the equine tuber coxae. (c) Histological assessment of new bone (*) within the MgPSr-PCL30 scaffolds after 6 months. Representative haematoxylin and eosin, basic fuchsin/methylene blue-stained MMA samples, immunohistochemical staining for collagen type I (brown region), and picrosirius red–stained tissue sections of defects filled by MgPSr-PCL30 scaffolds (S) and of empty defects. The scale bar is 50 μm. Adapted from [35].

ALP activity compared to control scaffolds after 7 and 14 days of *in vitro* culture [112].

Bone morphogenetic protein 2 (BMP-2) belongs to the transforming growth factor superfamily and plays an important role in bone regeneration [166]. Numerous studies have reported the use of BMP-2 to repair critical size bone defects; however, a carefully designed delivery system is critical to avoid adverse events, such as ectopic bone formation [82,83]. In a study conducted by Wang et al. [113], a HAp scaffold was first obtained via 3D printing and then coated with collagen/chitosan microspheres loaded with BMP-2 to obtain continuous growth factor release. After 8 weeks of *in vivo* implantation, ectopic bone formation was observed only in the HAp scaffold coated with BMP-2 [113]. Meanwhile, 3D printed mesoporous silica (MS)/CaP cement-based scaffolds loaded with BMP-2 showed increased bone formation and angiogenesis compared to BMP-2 lacking control scaffolds [114]. In addition to growth factors, alternative therapeutic drugs have been incorporated into 3D printed scaffolds. In a study by Bekisz et al., the local delivery of dipyridamole using 3D printed β-TCP/HAp scaffolds in a highly translational sheep calvarial defect model led to significant new bone [115].

Cell-laden scaffolds

Over the last decade, 3D printing technologies have received substantial consideration due to the remarkable disruptive potential in regenerative dentistry by providing personalised solutions to reconstruct dental, oral, and craniofacial tissues compromised by trauma, disease and/or congenital deformities [14,27,28]. Nonetheless, to satisfy tissue-specific needs it is important to imitate the biologic and functional hierarchy of the native tissues. In this way, bioprinting has materialised as a new and innovative 3D printing method for the generation of biologically functional tissue constructs with pre-programmed structures and patient-specific geometries. Bioprinting is defined as cell-laden biomaterial printing with precise positioning of cells into three-dimensionally organised structures using computer-aided layer-by-layer deposition [167]. Noteworthy, well-defined and geometrically complex structures laden with single or heterogenous cell populations can be realised to generate constructs physiologically and morphologically similar to relevant living tissues [168]. To date, depending on the cell type and bioink composition, extrusion-based bioprinting techniques have resulted in cell viability ranging from 80% to 90% within the bioprinted construct [13,31,120,123,169]. Hydrogel precursors are commonly used as bioink because they can provide a highly hydrated and permeable 3D polymeric structure that affords improved nutrient and oxygen diffusion, and thus enhancing cell survival and function [170]. In essence, hydrogels provide an ECM-like microenvironment, and can be tuned to enable cells to preferentially migrate within the hydrogel structure, unlike in native ECM [119,171,172].

Recently, cell-laden hydrogels modified with carefully selected growth factors have been deployed as highly translatable bioprinting strategies to generate vascularised bone tissue constructs with a high degree of reproducibility [36,123]. For instance, a pneumatic dispensing system was used to print bone marrow-derived MSCs (BMSCs) embedded in Poloxamer 407 and alginate [120]. There was no significant decrease in cell viability upon printing when compared to the non-printed cell-laden hydrogel counterparts. After

2 weeks, 3D bioprinted BMSCs expressed early markers of osteogenic differentiation, indicating that the printed cells were able to differentiate within the constructs following *in vitro* culture [120].

Traditionally, the combination of hydrogel with bioceramic is encouraged as the closest replicate of the extracellular matrix (ECM) composition of native bone [173]. Moreover, the incorporation of bioceramics into hydrogels has the ability to augment the bioactivity of the loaded cells [174,175]. As an example, a composite scaffold was devised by the combination of printable CaP cement, together with a cell-laden bioink consisting of 3% alginate and 9% methylcellulose (MC) [36]. There was no difference in cell viability between pristine alginate/MC scaffolds compared to CaP-modified bioprinted constructs. More importantly, after 7 days of *in vitro* culture, human MSCs started to migrate from alginate/MC bioink towards CaP cement strands [36]. Moreover, a model of osteochondral tissue grafts was fabricated by combining CaP cement, alginate/MC, and biphasic scaffold (consisting of CaP cement and alginate/MC bioink) [36]. In a different study, Kim and colleagues proposed cell-laden β-TCP and collagen hydrogels using a two-step printing process. Briefly, micron-sized α-TCP/collagen struts were printed to provide a mechanically stable structure, upon which a cell-laden collagen bioink was bioprinted onto the α-TCP/collagen struts. The composite scaffold showed significantly higher cellular activities compared to the cell-laden collagen scaffolds (Figure 12(a)) along with improved osteogenic differentiation (Figure 12(b)) [31].

As previously alluded to, the modification of bioinks with growth factors has been shown to significantly heighten osteogenesis [82,96,112]. BMP-2 serves as an important growth factor for bone regeneration; however, its halflife in the body is extremely limited and has some key safety concerns that are currently far from being addressed [176]. To surmount this drawback, our group developed a bioink that combines micron-sized amorphous magnesium phosphate (AMP) particles and an extracellular matrix (ECM) hydrogel containing 2% octapeptide FEFEFKFK (F/phenylalanine; E/glutamic acid; and K/lysine) and 98% water with excellent printability and shape fidelity. The encapsulated cells in AMP-modified bioprinted constructs showed elongated morphology and viability similar to AMP-free hydrogel (Figure 12(c)). Notably, cell-free AMP-laden constructs demonstrated increased bone formation when implanted in calvarial defects for 8 weeks when compared to the AMP-free constructs, indicating AMP's chemical ability to trigger osteogenic differentiation of endogenous cells surrounding the bone defect (Figure 12(d)) [13]. In a similar study, the incorporation of β-TCP particles into a collagen-based bioink led to 3D constructs with improved
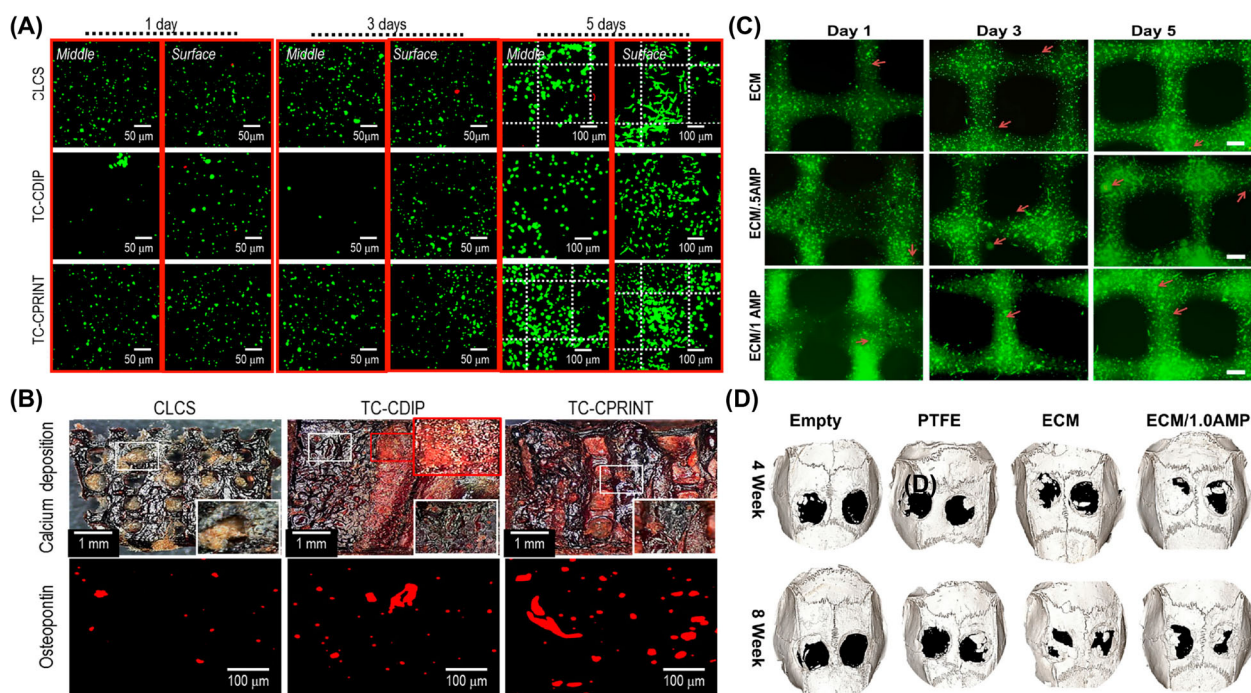
Figure 12. (a) *In vitro* cell-activities and live/dead images of the cell-laden scaffolds. (b) Osteogenic activities (Alizarin Red S and Osteopontin staining) of cell-laden scaffolds at day 14. Adapted from [31] (c) Calcein AM (green) and PI (red) staining assay for live and dead analysis of DPSCs after 1, 3, and 5 days in the cell-laden ECM and ECM/AMP-bioprinted constructs (red arrows: dead cells). DPSCs show an elongated morphology in AMP-modified constructs. (d) Micro-CT analysis of rat skull 3D rendering at 4- and 8-weeks. Calvarial defects that were left empty did not heal spontaneously for the duration of the study. In contrast, bone healing was gradually achieved when the defects were filled with either ECM or ECM/1.0AMP. Adapted from [13].
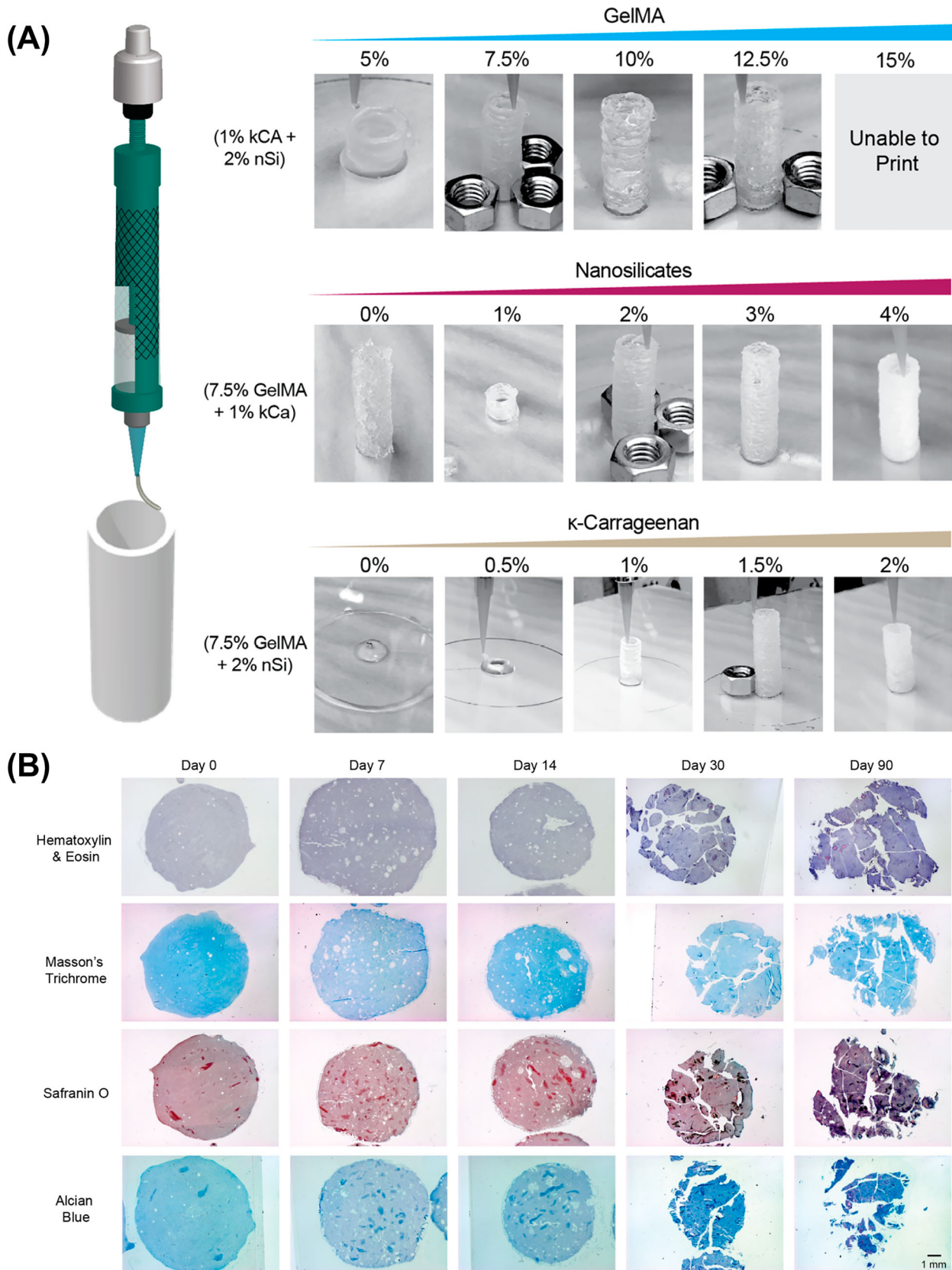
Figure 13. (a) The 3D printability of each NICE bioink formulation was quantified using screw-driven extrusion printer to fabricate a 3 cm tall, 1 cm wide hollow tube. (b) Histology show progressive changes in the ECM of 3D bioprinted structures. Masson trichrome (bone tissue) Safranin O (cartilage tissue) Alcian Blue (connective tissue). Adapted from [122].

stiffness and enhanced osteogenic differentiation of encapsulated adipose stem cells [121].

The translation of cell-printing technologies to preclinical and clinical models is still challenging due to the decreased shape fidelity of cell-laden constructs post-printing. To overcome this challenge, nanoengineered ionic covalent entanglement (NICE), a covalently crosslinkable gelatin methacryloyl (GelMA);

ionically crosslinkable kappa-carrageenan; and electro-statically charged nanosilicates were used to formulate a novel bioink (Figure 13(a,b)). The 3D printing of hMSCs encapsulated in growth factor-free conditions showed osteo-related mineralised ECM (Figure 13(c, d)) [122]. Hence, it is expected that cell-laden bioprinting can result in the development of tissue constructs with structural integrity and clinically relevant anatomical geometries for craniofacial bone and periodontal regeneration.

Collectively, the aforementioned findings show, that extrusion-based bioprinting can render scaffold or tissue constructs with prominent shape fidelity. Remarkably, a variety of printhead designs can be used to load and print diverse materials to ensure control in terms of biological, physicochemical, and mechanical properties. The spatiotemporally controlled release of growth factor(s) from 3D bioprinted constructs and the incorporation of vascular-like channels demonstrated the potential therapeutic benefit of regenerating large bone defects with improved vascularisation. The simultaneous printing of multiple materials using distinct extrusion-based methods can facilitate the engineering of scaffolds with compositional and structural gradients to mimic native tissues and tissue interfaces. Moreover, extrusion-based bioprinting has resulted in adequate cell survival and function, particularly within small

bone tissue constructs. In sum, extrusion-based bioprinting has made sizeable advances in the development of *in vitro* model systems and *in vivo* therapeutics with translational potential for applications in craniofacial bone and periodontal tissue reconstruction.

Convergence bioprinting technologies for fabrication of architecturally complex constructs

Living tissues are architecturally complex structures with different cells and matrices arranged in three dimensions, and thus engineering of bone and periodontal tissues to replace damaged tissues demands a tissue-specific and personalised approach. In this sense, the dynamics of 3D printing and bioprinting technologies have enhanced the perspective for complete regeneration of craniofacial bone and periodontal tissues through the fabrication of defect-specific designs to mimic structure(s) damaged or lost due to trauma, resection, or chronic inflammatory diseases, such as periodontal disease.

A leading approach for the reconstruction of highly organised living tissues and tissue interfaces, resides in the convergence of complementary 3D printing/bioprinting technologies integrated into a single biofabrication platform, recently termed multitechnology
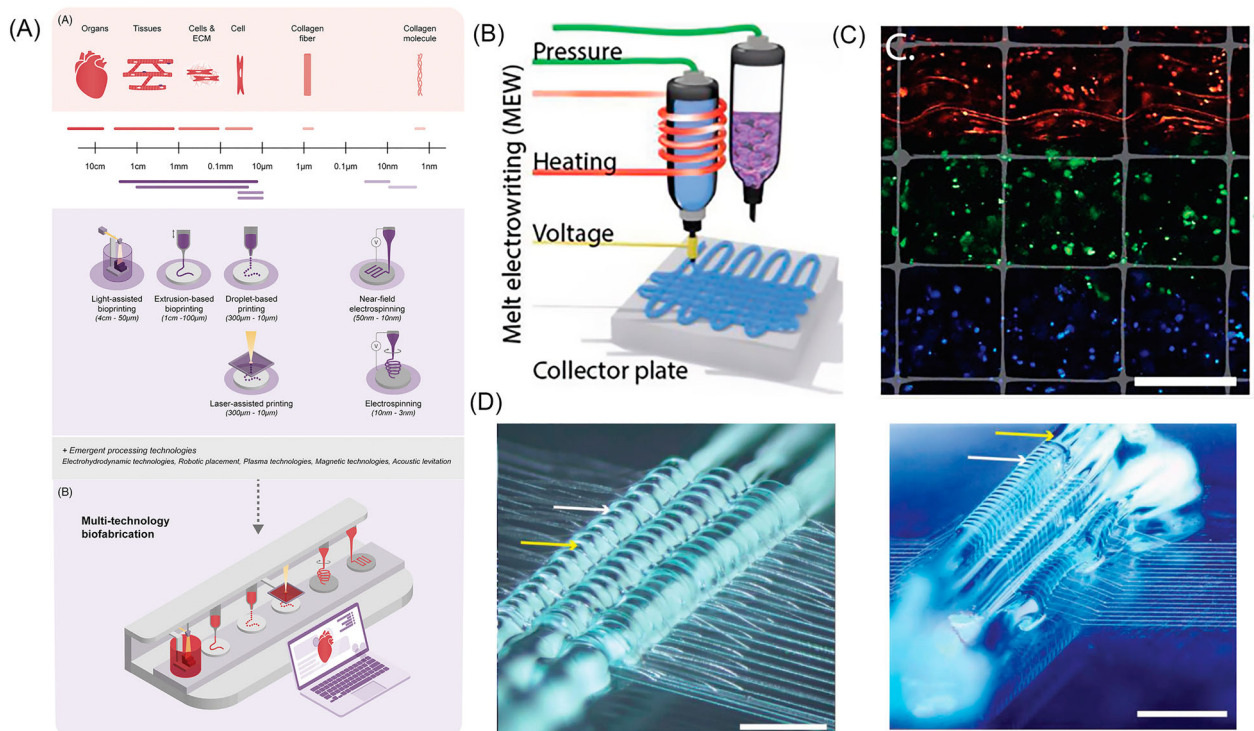
Figure 14. (a) Schematic Illustration of multitechnology biofabrication showing typical operation length of single deposition biofabrication technologies with the size and hierarchical structure of tissues and organs. Adapted from [40] (b) Convergence of MEW (PCL) and extrusion-based bioprinting (GelMA) into a single-step approach. (c) Fluorescence staining showing spatial placements of the cells in the composite constructs. (d) The guidance of MEW fibres over a strand of hydrogel for development of complex tissue architectures I) interlocked with hydrogel, and II) out-of-plane fibre deposition. Yellow arrows depict the hydrogel whereas the white arrows depict the PCL fibre. Scale bar = 500 μm Adapted from [38].
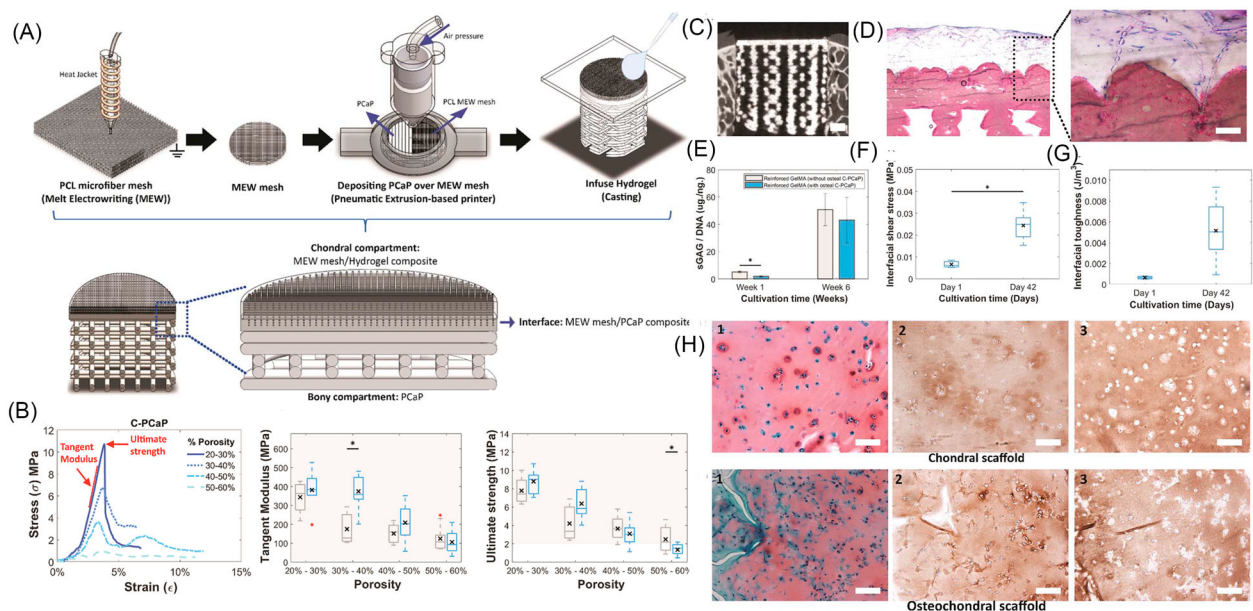
Figure 15. (a) Fabrication process of the osteochondral construct by using a combination of different 3D printing techniques. (b) Mechanical properties of the biomimetic PCaP scaffolds. (c) Micrograph obtained from micro-CT scanning showing a biomimetic PCaP scaffold that could be placed press-fit inside an ex vivo osteochondral defect (scale Bar = 1 mm). (d) Basic fuchsin and methylene blue staining reveal pattern of embedded PCL microfibres inside the non-porous layer of the C-PCaP scaffold of the constructs with osteal C-PCaP anchor. (Scale Bar = 100 μm). (e) Quantification of sGAG in hydrogel per DNA content. (f) Interfacial adhesion strength, and (g) interfacial toughness (day 1 and day 42) while applying shear force at the interface between equine ACPCs encapsulated in GelMA and C-PCaP-based bone compartment. (h) Safranin-O staining (1), collagen type II immunostaining (2) and collagen type I immunostaining (3) of paraffin embedded microfibre reinforced GelMA without osteal C-PCaP (F) and with osteal C-PCaP (G), respectively, after cultivation for 42 days. (Scale Bar = 100 μm). Adapted from [132].

fabrication (Figure 14(a)). Converged biofabrication has the potential to yield scaffold systems with high printing fidelity, spatial control over cell distribution and improved biomechanical properties without compromising cell viability and functionality [40]. For example, successful combined approaches of hydrogel printing and electrospinning or MEW of polymers have already been reported [38,177]. In addition, Xu and colleagues pioneered the combination of inkjet bioprinting with solution electrospinning to fabricate cartilage tissue constructs [177]. By alternating the deposition of electrospun polycaprolactone/pluronic fibre meshes and inkjet printed chondrocytes containing hydrogels, the authors were able to create a series of millimeter-sized constructs with promising biomechanical properties and encouraging cartilage-like tissue formation. More recently, de Ruijter and co-authors shown the successful combination of extrusion-based bioprinting and MEW in a single biofabrication platform, which allowed for the generation of living constructs with the spatial distribution of mesenchymal stromal cells and improved biomechanical functionality without jeopardising cell viability or chondrogenic differentiation (Figure 14(b–d)) [38]. In a follow up study Diloksumpan and colleagues demonstrated another promising converged biofabrication strategy to engineer hard-to-soft tissue interfaces (Figure 15(a–h)) [132]. Altogether, the integration of fibre technologies with cell printing

enhances the mechanical competences of the bioprinted constructs while simultaneously offering cues for (stem) cells to differentiate and organise tissue matrix. In a study focus on the hard-to-soft periodontal tissue interface, an osteoconductive biphasic scaffold with a bone compartment was fabricated using β-TCP/PCL printed via FDM, then coated with CaP and the periodontal compartment was electrospun through a melt electrospinning device (Figure 16(a)). *In vivo* analysis confirmed the integration of tissue between the two compartments and the formation of structurally similar tissue to native periodontal tissues (Figure 16(b,c)) [178].

Alongside this strategy, other combinatorial approaches consisting of extrusion-based printing integrated with sacrificial support materials [179], external magnetic field stimulation [180,181] or atmospheric plasma functionalisation [182] have been described. Such strategies have the potential to generate personalised biologically relevant tissue-like materials with relevant sizes and structures that were previously deemed as 'unprintable', while affording high cell viability. These biofabrication platforms can also provide suitable mechanical and structural features to direct cell growth and differentiation. An even more enticing feature of this fabrication systems is the combination of digital design tools coupled with multitechnology biofabrication to create materials with locally defined chemical compositions,

structures, and properties that can resemble biological materials and ultimately drive tissue regeneration [40]. We strongly believe, this next generation of multitechnology biofabrication systems will incorporate real-time inline monitoring of the printing process through combinations of machine vision, inspection sensors, and feedback control systems supervised by artificial intelligence (AI) algorithms for high-throughput and truly functional tissue equivalents biomanufacturing [40].

It is worth noting that the hierarchically organised bone and connective tissues also present micro-vascularisation and innervation that should be replicated while generating scaffolds for bone and periodontal tissue engineering. Although mimicking bone microvasculature and innervation is usually neglected in regenerative therapies, recent publications have directed their focus over to these very sensitive matters for successful clinical translation of bone tissue analogs [133,138,140]. For instance, tuning β-TCP scaffolds with 5% calcium-silicate and loading the 3D constructs with co-cultures of HUVECs and human bone marrow-derived stem cells (hBMSCs) induced vessel formation through the porous structure of the scaffolds and new bone tissue in rat models [133]. The authors also highlighted that the revascularisation process contributed to the supply of biomolecules involved in bone tissue regeneration. Meanwhile, another significant gain in vascularised tissue during bone regeneration was achieved by 3D printing PCL-Chitosan-deferoxamine scaffolds [140]. Deferoxamine (DFO) promotes hypoxia conditions, which apparently plays a role in the modulation of genes key to angiogenesis and osteogenesis. In this way, 3D printed scaffolds modified with DFO led to the upregulation of essential genes related to vascularisation and mineralisation and induced high vascular volume and bone formation in femoral defects [140]. Regardless of the important findings of vascularisation- and bone regeneration-inductive mechanisms, these studies printed porous constructs involving no specific architecture, and the innervation aspect was not taken into account.

Remarkably, in a recently published work, the unique architecture of Haversian bone was successfully mimicked using 3D printing for multicellular delivery in bone regeneration [138]. Bioceramic-based scaffolds were printed by digital laser processing (DLP) with different pore sizes and arrangements that replicate cancellous bone, Haversian, and Volkmann canals within a single construct, as evidenced in natural bone and by the amount and distribution of the channels, as the volume of cortical bone determined the strength of the scaffolds. The co-cultures of osteogenic and angiogenic or neurogenic cells were effective in proliferating and expressing specific markers of mineralisation, vascularisation, and innervation. Noteworthy, upon *in vivo* implantation the fabricated scaffolds induced new bone formation, following the design of the construct, and the endothelial cells cultured into the Haversian canals accelerated vessels' ingrowth through the construct [138]. However, the proposed co-cultures' model still needs to be checked *in vivo*, including osteogenic, neurogenic, and vasculogenic cells in a single model to validate the findings. Nonetheless, the gradually arranged and highly complex architectures present in that scaffold reinforce the remarkable advances 3D printing technology has brought to the dynamics of regenerating bone.
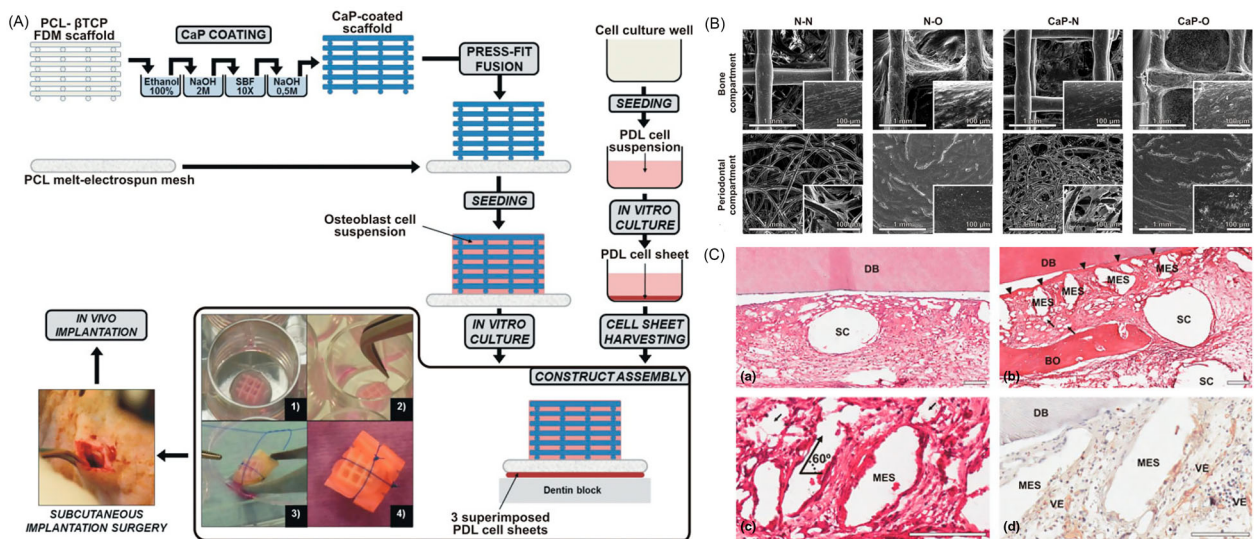
Figure 16. (a) Graphical illustration of the biomimetic coating procedure, the fabrication of the biphasic scaffold, cell seeding, subsequent in vitro culture and in vivo implantation of the cellular constructs. (b) SEM images of the seeded scaffolds after 6 weeks of *in vitro* culture under four different conditions. N–N non-coated scaffold cultured in basal medium, N–O non-coated scaffold cultured in osteogenic medium, calcium phosphate–N calcium phosphate-coated scaffold cultured in basal medium, calcium phosphate–O calcium phosphate-coated scaffold cultured in osteogenic medium. (c) Representative H&E and immunostaining images of implanted biphasic scaffolds. Adapted from [178].
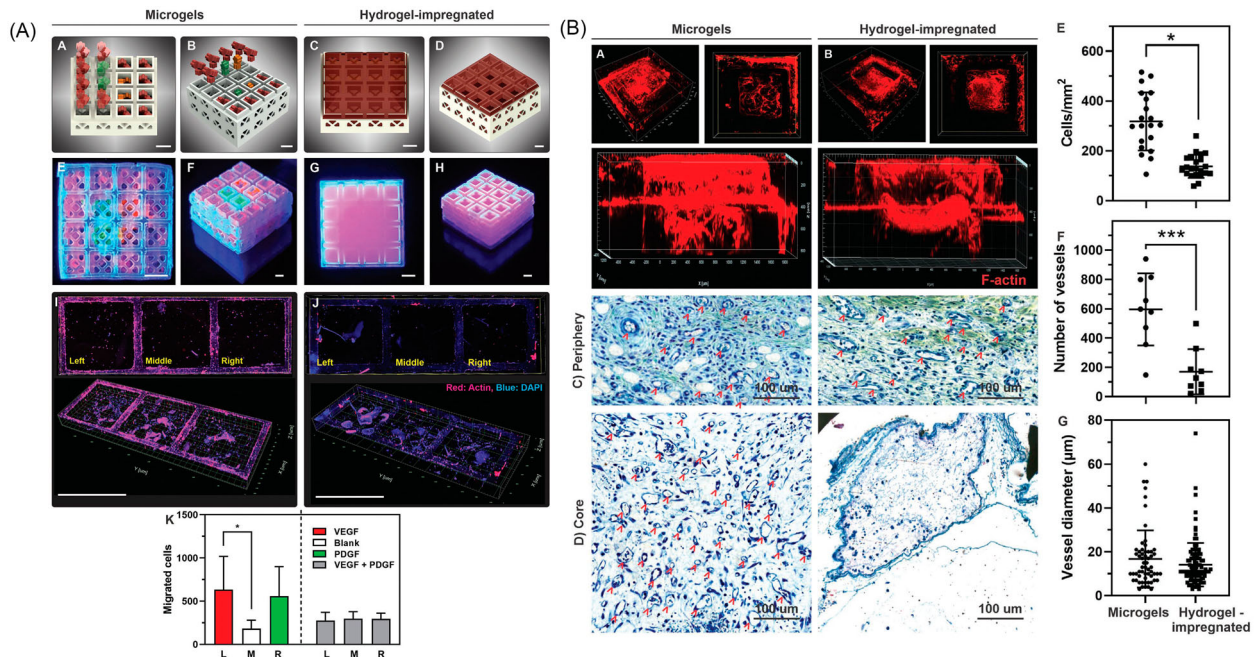
Figure 17. (a) (A-D) 3D diagram showing the distribution of microgels and impregnation of hydrogel in individual microcage units. (E-H) Photographs of the microcage scaffolds schematically depicted above after loading with fluorescently labelled microparticles embedded with the microgel and monolithic hydrogel. (I-K) Transwell migration assay shows distinct migration toward the microcages as confirmed by the immunofluorescence staining images (top: 2D view, bottom: 3D view) and Corresponding quantitative data of cells migration ($p < 0.05$) (scale bar: 1.5 mm). (b) (A-B) Angled, top, and orthogonal projections of F-actin-stained samples show the infiltration of cells throughout the microgel-loaded microcage scaffolds in comparison with the hydrogel-impregnated samples. (C-G) Histology (toluidine blue staining) images, quantification of cell distribution and vessel diameter show directed cell migration and neovascularisation (indicated by arrowheads) in the periphery and core regions of the microgel-loaded microcage scaffold, when compared with the hydrogel-impregnated samples, which showed little evidence of cellularity and vasculature formation in the core regions. Adapted from [134].

Latest research 3D printed the stackable miniaturised microcage modules, resembling the features of toy interlocking building blocks (e.g. LEGO) loaded with different growth factors, such as VEGF, PDGF, and BMP2 to create a concentration gradient within the microcage scaffold to direct cell migration in specific fashion. Lithography-based Ceramic Manufacturing (LCM) 3D printing technique, was used to create 1.5 mm microcages with wall thickness of 230–560 μm. Digital Light Processing (DLP) 3D printing was used to build five-pointed flower-like geometry loaded with growth factors which was manually placed inside the microcage. The study found that the infiltration of cells was 2-fold greater and vascularisation was 3-fold higher in microgel-loaded microcage modular scaffolds than hydrogel-impregnated composite scaffold (Figure 17(a,b)) [134].

Craniofacial bone injuries can occur throughout the lifetime of a patient. Hence, it is critical to ponder the age and stage of bone development when planning a regenerative-based therapy. Also, congenital anomalies, such as orofacial clefts, imply special approaches and knowledge regarding tissue development and growth. Accordingly, advances in the field were recently achieved using 3D printed scaffolds as a concept extrapolation for regeneration at different stages of bone growth [125,135]. For instance,

β-TCP scaffolds loaded with dipyridamole, an osteoinductive drug, were previously tested in calvaria [115] and to regenerate long bone defects [137]. The 3D printed scaffolds coated with dipyridamole [125] led to bone formation throughout the scaffolds' porosities, regardless of pore dimensions, and preserved suture patency for therapeutic and super-dosages of the osteoinductive drug [125]. Moreover, dipyridamole-loaded scaffolds induced native bone-like formation *in vivo* [135], and there was neither ectopic bone formation nor scaffold-induced asymmetry, and the bone sutures were not affected by the bone regeneration process (Figure 18(a–c)) [135]. Since suture patency preservation is relevant to maintaining normal development of the craniofacial skeleton, these studies informed an important path on the use of 3D printing for bone regeneration when considering different stages of life and bone growth. However, these experiments were not tested in a real craniofacial cleft defect. Ideally, that type of analyses should map the real defect based on 3D images to be converted into defect-specific constructs.

The periodontium forms an important complex and comprises multiple tissues (i.e. gingival, cementum, periodontal ligament, and alveolar bone) at distinct locations that act together to allow the tooth to be attached to the jaw and to afford a defensive barrier
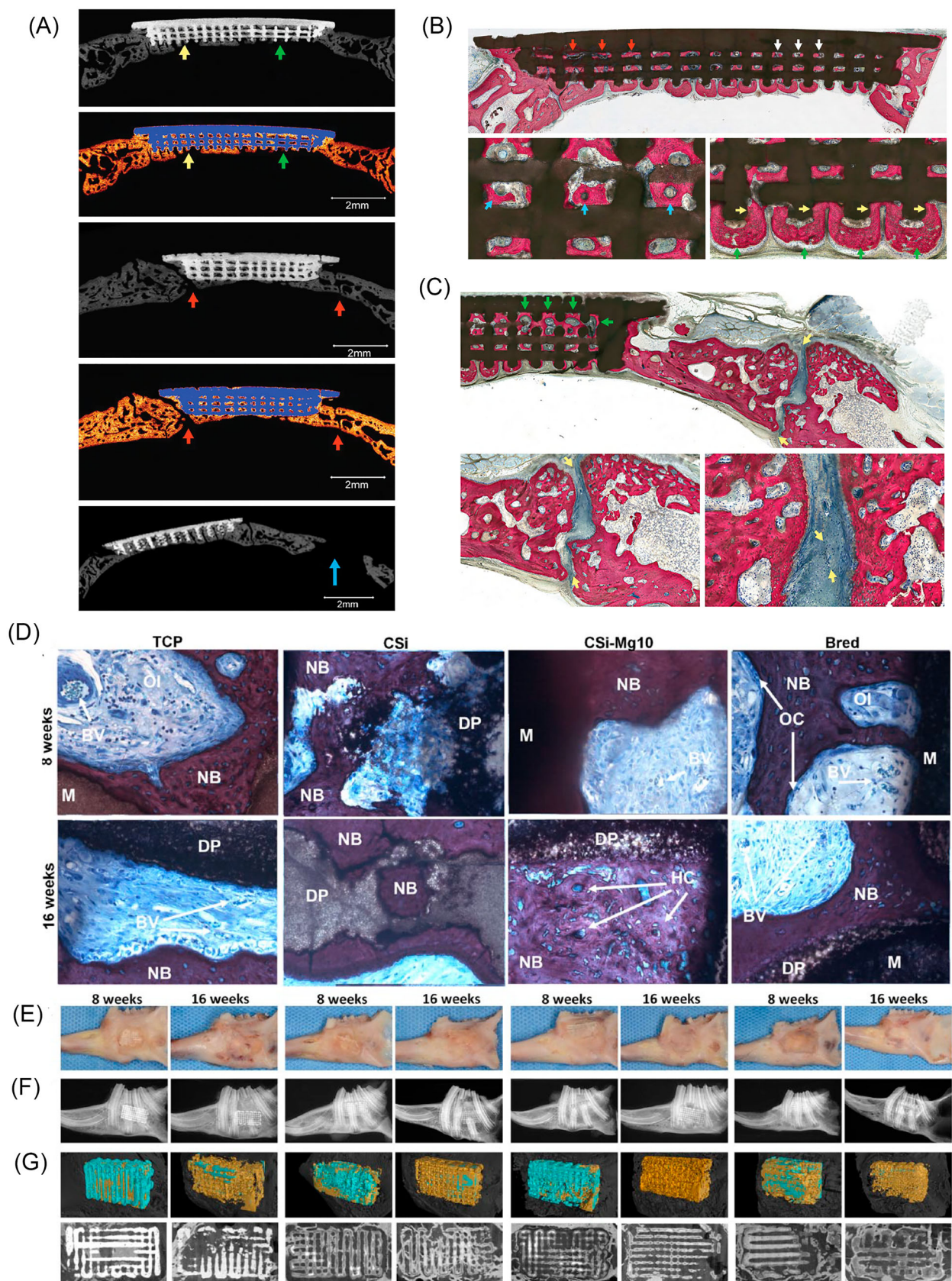
Figure 18. (a) Micro-computed tomographic slices of new bone formation within scaffold at 8 weeks. The osseoconductive infiltration through the scaffolds (green and yellow arrows on second row) and bone regeneration in immature skeletal calvaria did not affect the suture patency (red arrows). (b-c) Histological examination showing bone formation is guided by highly osseoconductive scaffold dimensions as new bone formation is directed from scaffold pore-to-pore while interacting with scaffold struts. Adapted from [125]. (d) Histological analysis of bone defect site in rabbit mandibles, ×20 (e) Images of the specimens. (f) Radiographs of the specimens. (g) Two-dimensional, 3-dimensional micro-computed tomography (CT) images of the scaffolds implanted in the rabbit alveolar defects with different time separately. Adapted from [117].

for the underlying structures from the oral microflora. In order to overcome the challenges in regenerating multiple tissues, hydrogel-based scaffolds must contain a heterogeneous cell population at predesignated sites with a high degree of spatial organisation [183] to allow the fabrication of a multitissue structure comprising bone and mineralised cementum-like core enclosed within a periodontal ligament (PDL)-like tissue. An innovative approach, with significant potential in periodontal tissue regeneration, was successfully deployed using a multi-head tissue/organ building system (MtoBS) with 6 dispensing units for the biofabrication of cell-laden constructs for osteochondral tissue regeneration. The multilayered living constructs containing human turbinate-derived mesenchymal stromal cells (hTMSCs) and growth factors was printed in the empty cavity of a predesigned biodegradable polymer (PCL) framework. The hTMSCs were embedded in a hydrogel comprised of atelocollagen and supramolecular hyaluronic acid to give rise to subchondral bone, and a superficial cartilage layer, respectively [37]. In addition, transforming growth factor (TGF)-β and rhBMP-2 were added to atelocollagen and supramolecular hyaluronic acid, respectively. PCL fibres were extruded from a heated nozzle of MtoBS, an in-house-developed 3D printing system. A cell-rich cylindrical 3D construct 5 mm in height was divided into a 4 mm subchondral bone layer and a 1 mm cartilage layer and was implanted into the osteochondral defect in the knee joint of a rabbit. Macroscopically, the defect was fully covered after 8 weeks with neo-tissue, exhibiting a smooth surface, and the cartilage-like neo-tissue was whiter than the adjacent native cartilage. However, cell-seeded PCL scaffolds partially covered the defect, and neo-tissue was primarily found in the interface between the native tissue and the defect [37].

Over the last decade, promising steps to realise tissue-specific and geometrically complex constructs have been possible through the combination of high-resolution images from 3D computed tomography (CT) and computed software available for 3D printing, which has fostered new horizons on the development of personalised scaffolds for regenerative medicine. This combination has been used for many years by prototyping bone implants. Now, the conversion of CT images into defect-specific scaffolds has also instigated novel therapies and biofabrication approaches, for craniofacial bone and periodontal tissue regeneration [117,184]. For example, mineralised collagen-loaded porous titanium scaffolds were designed based on CT images of rabbits' large bone defects [184]. The porous structure of titanium and the collagen embedded in the scaffolds not only induced new bone formation and osseointegration, but also stimulated the expression of angiogenesis markers through the porosities [184]. Despite osseointegration

and biocompatibility properties, titanium constructs are not degradable. Thus, this type of construct is directed to weight-bearing and large bone defects' reconstruction. Regarding craniomaxillofacial bone defects, digital images from 3D microfocus CT were used to obtain defect-specific bioceramic constructs for repairing mandibular defects [117]. Wollastonite scaffolds modified 10% Mg induced bone regeneration throughout the entire defect after 16 weeks and a reasonable degradability ratio. These scaffolds were also more efficient as a regenerative material than other CaP-based constructs (Figure 18(d–g)) [117]. These bone-regeneration outcomes were achieved in controlled defects from sound tissue models, without infection, which makes this type of construct suitable for treating fractures and resections. However, it is hard to predict the behaviour of these constructs as facing possibly infected niches like it can occur in periodontal defects. Therefore, while printing cells and/or personalised constructs, drugs can also be incorporated into the system to minimise inflammation of surrounding tissue to allow for healthier bone growth [185]. For instance, osteoblasts-laden alginate-based hydrogels containing diclofenac, an anti-inflammatory drug, were bioprinted using a pneumatic system. The alginate scaffold was coated with 1% chitosan scaffold to control release of diclofenac from the bioprinted construct. Taken together, the study confirmed that diclofenac suppressed secretion of inflammatory compounds and resulted in enhanced cell proliferation and calcium secretion [124].

From a detailed dental perspective, periodontium comprises protective and supportive structures, and its interactive function is important for maintaining oral health. Furthermore, periodontal structures involve hard (alveolar bone and cementum) connective tissues (periodontal ligament) and their interfaces, which makes the design of personalised and defect-specific 3D constructs a challenge for the simultaneous and coordinated growth of hard and soft tissues. Theoretically, ideal constructs for periodontal tissue regeneration should present a certain level of compartmentalisation, because of differences in size, arrangement, type of cells, and structural properties of the three (i.e. cementum, periodontal ligament, and alveolar bone) components of the supportive periodontium. At the same time, the system works as a bundle that cannot be dissociated, and their interfaces micron-scale organisation and transitions are more complex to replicate and demand very accurate 3D printing technologies. Therefore, over the last decade, the development of scaffolds to guide periodontal ligament fibres' alignment and proper insertion is a relevant approach to mimic the native conditions of periodontal tissues has been systematically investigated. For instance, the periodontal ligament (PDL) attaches to bone and cementum and plays an
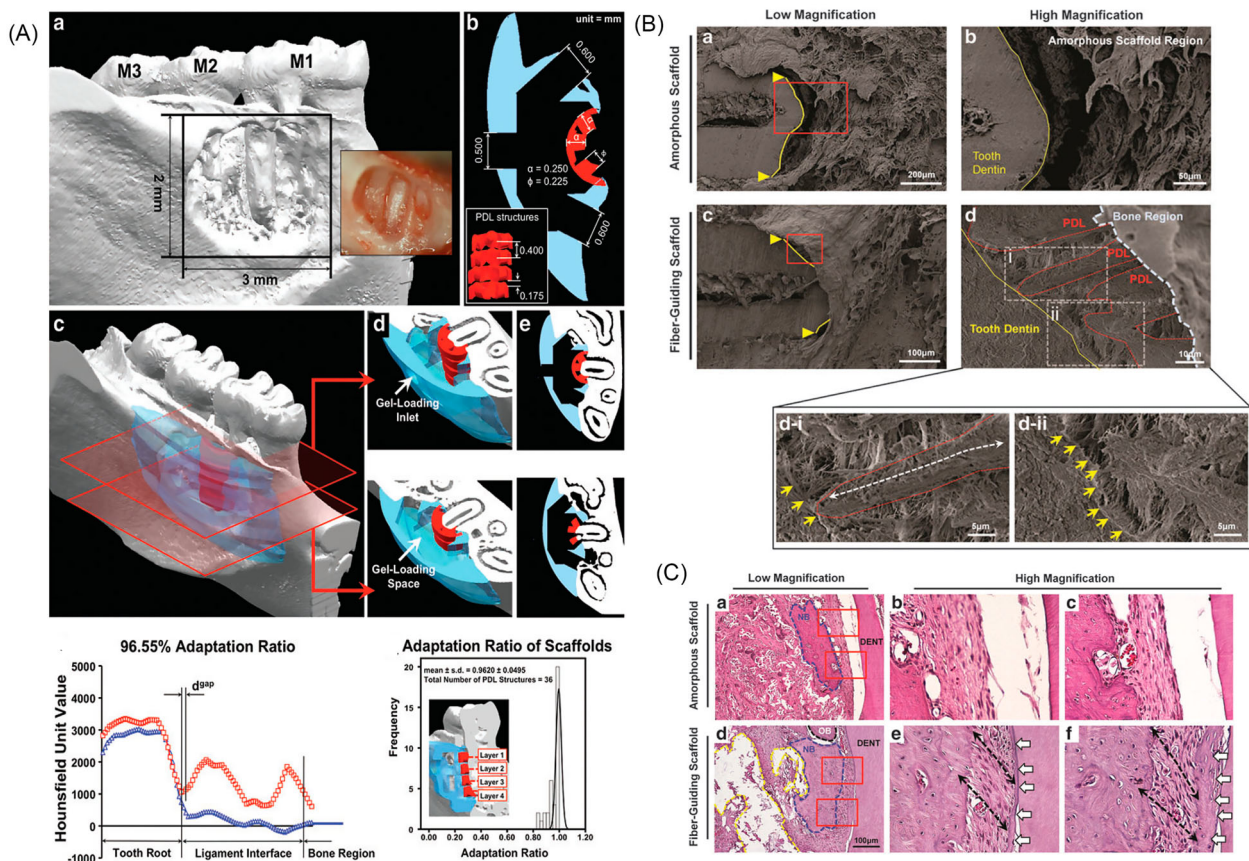
Figure 19. (a) Micro-CT images of a periodontal defect and the design and adaptation ratio of a site-specific scaffold for regeneration. (b) SEM images evidencing dense formation of fibrous tissue for the fibre-guiding scaffolds and collagen-like fibres anchorage on the dentin structure. (c) Histological analysis (H&E) comparing tissue morphologies and organisation of random and fibre-guiding scaffolds. Adapted from [186].

important role in biomechanical load distribution and proprioception. Each group of fibres of the PDL has a specific alignment contributing to masticatory and bite force dissipation, while it controls tooth movement and stability. Thus, controlling the fibre deposition and space between layers has fostered the development of 3D printing methods that can fabricate accurate scaffolds that replicate not only the micron-scale, but also the geometries of specific periodontal defects.

From this viewpoint, it is noteworthy that different 3D printing techniques have been purposed to develop scaffolds for PDL regeneration, but feasibility and clinical translation of these methods are still limited [126,136,186,187]. Initial achievements were mostly based on the use of CT images to aid accurate size and orientation, while designing the constructs. For instance, cone-beam CT (CBCT) images from the periodontal defects of rats were used to create 3D designs with structural integration among components of supportive periodontal tissues, and, subsequently, freeze-casted PCL constructs were synthesised from those designs to guide regeneration and PDL fibres' orientation [186]. The constructs had a high adaptation ratio to the defect,

while the same constructs loaded with human PDL cells (hPDL) and fibrin gel induced PDL fibres' regeneration and proper orientation, and the bone part of the construct induced new bone formation (Figure 19(a–c)).

Another interesting aspect about the PDL is that it presents different micron-scale organisation according to the region of the root where it attaches. To address that specificity, micro-grooved 3D patterns were developed to guide PDL fibres formation [126,136]. The freeze-casted PCL micro-grooved constructs induced PDL cells' alignment at different angles (0°, 45°, and 90°) (Figure 20(a,b)) [136]. Also, these studies reinforced that the scaffolds and polymer nature-related factors, such as depth and roughness of the constructs, influence the organisation of newly formed tissue *in vivo* [126,136]. On one hand, designing angulated micropatterns for guiding PDL regeneration encourages further research. On the other hand, removing the construct from the mould when using this more simplistic casting-assisted approach is a very sensitive procedure and minimal errors in that step could compromise the integrity of the scaffold.

Fortunately, other 3D printing technologies have been identified to design and print these complex
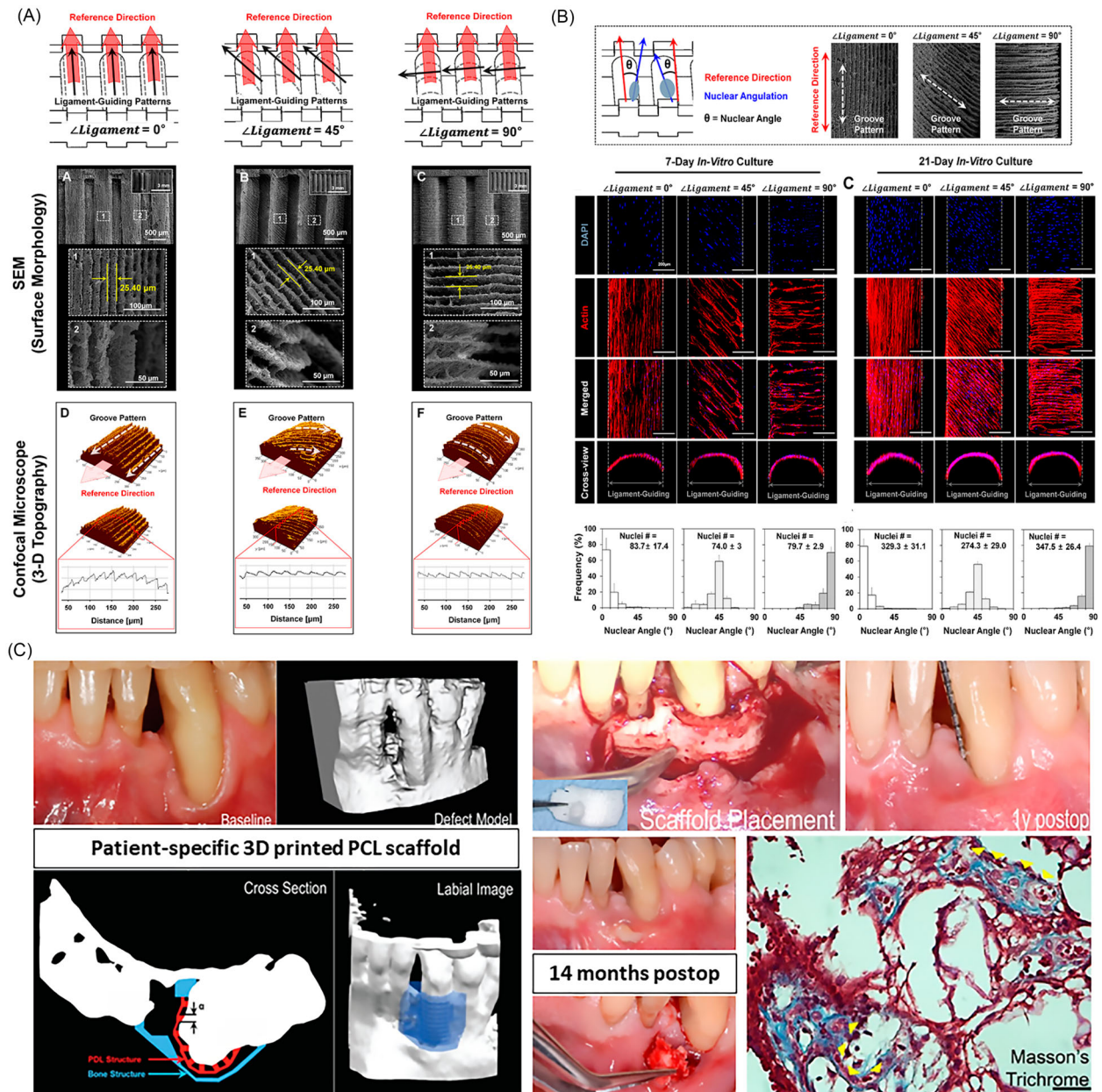
Figure 20. (a) Micro-groove pattern designs to guide PDL orientation (0°, 45°, and 90°). SEM and confocal microscopies illustrates surface morphology and topography of the constructs according to the micro-groove orientation. (b) Fluorescence images and quantitative data for the cell and nuclear angulation of hPDL cells being influenced by the 3D micro-groove patterns after 7 and 21 days of culture. Adapted from [136]. (c) 3D printing using polycaprolactone was made to fit the periosseous defect based on the patient's cone beam computed tomography scan. The implanted 3D scaffold filled the periodontal osseous defect without clinical signs of chronic inflammation or rejection of the polycaprolactone-based material during the first year. After 14 months, due to postoperative exposure (i.e. soft tissue dehiscence over the scaffold), the patient-specific 3D printed scaffold was retrieved. Histologic analysis of the retrieved scaffold with Masson's trichrome staining indicates small islands of new bone formation within a milieu of primarily granulomatous tissue (yellow arrowheads). Scale bar = 50 μm. Adapted from [14].

periodontal tissue constructs. In this way, it is necessary to combine the most relevant findings of different research groups to develop prime 3D printed scaffolds for clinical translation. To date, there is a single clinical report in the literature that uses CBCT images to create a defect-specific 3D printed polymeric (PCL) scaffold for periodontal regeneration [14], designed using a selective laser sintering (SLS) approach to treat a large periodontal osseous defect [14]. Specifically, SLS was utilised to fabricate a HAp-modified

PCL-based composite scaffold according to the anatomical configuration of the defect. The scaffold was designed to display perforations for fixation, an internal port for delivery of recombinant human platelet-derived growth factor (PDGF-BB), and pegs perpendicularly oriented to the root to guide PDL formation. The adaptation ratio based on the methodology for PDL fibre guidance was defined based on micro-CT data. Before implantation, the scaffold was immersed in rhPDGF-BB, filled with autologous

blood, and stabilised over the defect with resorbable pins. No clinical signs of chronic inflammation or rejection associated with the presence of the scaffold was seen during the first 12 months. A burst release of rhPDGF-BB was observed within the first 3 h in an *in vitro* drug release study. From a clinical standpoint, the scaffold remained covered for 12 months, revealing a 3-mm gain of clinical attachment and partial root coverage. Regrettably, scaffold exposure was noticed at 13 months and, though palliative measures were completed to save the treatment, the implanted scaffold ($\sim$ 76% of its original molecular weight) was removed (Figure 20(c)) [14]. While the success of that clinical study was far from ideal, given that complete regeneration of the periodontium was not observed, it provided key information to drive the field forward, particularly regarding the aspects associated with scaffold design and fabrication.

Future outlook

Although 3D (bio)printing has been identified as a paradigm-shifting platform technology with real potential in delivering patient-specific and functional regenerative therapeutics in dentistry, it still remains in its infancy. Undoubtfully, future work in the development of personalised and functional scaffolds for craniomaxillofacial (CMF) bone and periodontal regeneration will continue to encompass high-resolution imaging (computed tomography) combined with printing technologies and biomaterials to recapitulate not only the tissue-specific architecture and function, but also to address the very challenging objective of rebuilding the different tissues and tissue interfaces found in the periodontium. To address these challenges, great efforts have been made to engineer defect-specific scaffolds mimicking the hierarchical and complex architecture of the periodontium.

Up to now, extrusion-based (bio)printing systems have shown great potential to design, using a variety of biomaterials, personalised scaffolds for CMF bone and periodontal tissue regeneration. Although this printing technology has been successfully applied to fabricate scaffolds/constructs loaded with tissue-specific cell types and/or biomolecules to amplify the predictability of the regenerative outcome; little attention has been given to antimicrobial and immunomodulatory strategies. Future work on the integration of antimicrobial drugs and/or biomaterials with immunomodulatory capability to enhance the regenerative response upon 3D (bio)printed scaffold implantation should be also explored.

In addition, ongoing improvements in 3D (bio)-printing of engineered vascularised and innervated analogous bone tissues are outlining as the future of regenerative oral and orthopaedic bone regeneration therapies. These developments will lay the groundwork for designing improved scaffolds and implants both from an anatomical and biological fidelity viewpoint. Nonetheless, concerns about successful and expeditious translation of 3D bio(printing) technologies for regenerative dentistry is dependent on the careful development of guidelines and standardisation of clinical protocols to accelerate the required approval from regulatory agencies, such as the FDA and CE. To reach this goal, future studies should broaden the concept of technology convergence by leveraging the fast-evolving 3D (bio)printing technologies (multimaterial bioplotters) and materials/bioinks to build physiologically relevant tissues and tissue interfaces to suitably reconstruct CMF bones and periodontal tissues. The successful translation of these concepts to clinics will support multiple possibilities of regenerative therapies and quotidian patient care.

ORCID

Zeynep Aytac http://orcid.org/0000-0002-6469-9653
Nileshkumar Dubey http://orcid.org/0000-0002-6664-1375
Arwa Daghrery http://orcid.org/0000-0002-8328-1818
Jessica A. Ferreira http://orcid.org/0000-0002-9669-4339
Isaac J. de Souza Araújo http://orcid.org/0000-0002-1795-8640
Miguel Castilho http://orcid.org/0000-0002-4269-5889
Jos Malda http://orcid.org/0000-0002-9241-7676
Marco C. Bottino http://orcid.org/0000-0001-8740-2464

References

[1] Zhang W, Yelick PC. Craniofacial tissue engineering. Cold Spring Harb Perspect Med. 2018;8(1):a025775.

[2] Futran ND, Mendez E. Developments in reconstruction of midface and maxilla. Lancet Oncol. 2006;7 (3):249–258.

[3] Genden EM, Okay D, Stepp MT, et al. Comparison of functional and quality-of-life outcomes in patients With and without palatomaxillary reconstruction. Arch Otolaryngol.–Head Neck Surg. 2003;129 (7):775–780.

[4] Ward B, Brown S, Krebsbach P. Bioengineering strategies for regeneration of craniofacial bone: a review of emerging technologies. Oral Dis. 2010;16(8):709–716.

[5] Peres MA, Macpherson LM, Weyant RJ, et al. Oral diseases: a global public health challenge. The Lancet. 2019;394(10194):249–260.

[6] Eke PI, Dye B, Wei L, et al. Prevalence of periodontitis in adults in the United States: 2009 and 2010. J Dent Res. 2012;91(10):914–920.

[7] Eke PI, Borgnakke WS, Genco RJ. Recent epidemiologic trends in periodontitis in the USA. Periodontol. 2000. 2020;82(1):257–267.

[8] Bottino MC, Pankajakshan D, Nör JE. Advanced scaffolds for dental pulp and periodontal regeneration. Dental Clinics. 2017;61(4):689–711.

[9] Kornman KS. Contemporary approaches for identifying individual risk for periodontitis. Periodontol. 2000. 2018;78(1):12–29.

[10] Reichert JC, Cipitria A, Epari DR, et al. A tissue engineering solution for segmental defect regeneration in load-bearing long bones. Sci Transl Med. 2012;4(141):141ra93–141ra93.

[11] Obregon F, Vaquette C, Ivanovski S, et al. Three-dimensional bioprinting for regenerative dentistry and craniofacial tissue engineering. J Dent Res. 2015;94(9_suppl):143S–152S.

[12] Dubey N, Ferreira JA, Daghrery A, et al. Highly tunable bioactive fiber-reinforced hydrogel for guided bone regeneration. Acta Biomater. 2020;113:164–176.

[13] Dubey N, Ferreira JA, Malda J, et al. Extracellular matrix/amorphous magnesium phosphate bioink for 3D bioprinting of craniomaxillofacial bone tissue. ACS Appl Mater Interfaces. 2020;12(21):23752–23763.

[14] Rasperini G, Pilipchuk S, Flanagan C, et al. 3D-printed bioresorbable scaffold for periodontal repair. J Dent Res. 2015;94(9_suppl):153S–157S.

[15] Shen C, Witek L, Flores RL, et al. Three-dimensional printing for craniofacial bone tissue engineering. Tissue Eng, Part A. 2020;26(23–24):1303–1311.

[16] Bottino MC, Thomas V, Schmidt G, et al. Recent advances in the development of GTR/GBR membranes for periodontal regeneration – a materials perspective. Dent Mater. 2012;28(7):703–721.

[17] Yang F, Both SK, Yang X, et al. Development of an electrospun nano-apatite/PCL composite membrane for GTR/GBR application. Acta Biomater. 2009;5 (9):3295–3304.

[18] Karring T. Regenerative periodontal therapy. J Int Acad Periodontol. 2000;2(4):101–109.

[19] Gentile P, Chiono V, Tonda-Turo C, et al. Polymeric membranes for guided bone regeneration. Biotechnol J. 2011;6(10):1187–1197.

[20] Jung RE, Fenner N, Hämmerle CH, et al. Long-term outcome of implants placed with guided bone regeneration (GBR) using resorbable and non-resorbable membranes after 12–14 years. Clin Oral Implants Res. 2013;24(10):1065–1073.

[21] Ramakrishna S, Fujihara K, Teo W-E, et al. Electrospun nanofibers: solving global issues. Mater Today. 2006;9(3):40–50.

[22] Greiner A, Wendorff JH. Electrospinning: a fascinating method for the preparation of ultrathin fibers. Angew Chem, Int Ed. 2007;46(30):5670–5703.

[23] Chen X, Liu Y, Miao L, et al. Controlled release of recombinant human cementum protein 1 from electrospun multiphasic scaffold for cementum regeneration. Int J Nanomedicine. 2016;11:3145–3158.

[24] Gümüşderelioğlu M, Sunal E, Demirtaş TT, et al. Chitosan-based double-faced barrier membrane coated with functional nanostructures and loaded with BMP-6. J Mater Sci: Mater Med. 2020;31(1):4.

[25] Yang F, Wolke J, Jansen J. Biomimetic calcium phosphate coating on electrospun poly(ε-caprolactone) scaffolds for bone tissue engineering. Chem Eng J. 2008;137(1):154–161.

[26] Elgali I, Turri A, Xia W, et al. Guided bone regeneration using resorbable membrane and different bone substitutes: early histological and molecular events. Acta Biomater. 2016;29:409–423.

[27] Carter S-SD, Costa PF, Vaquette C, et al. Additive biomanufacturing: an advanced approach for periodontal tissue regeneration. Ann Biomed Eng. 2017;45 (1):12–22.

[28] Zadpoor AA, Malda J.. Additive manufacturing of biomaterials, tissues, and organs. Ann Biomed Eng. 2017;45: 1–11

[29] Farag A, Hashimi SM, Vaquette C, et al. Assessment of static and perfusion methods for decellularization of PCL membrane-supported periodontal ligament cell sheet constructs. Arch Oral Biol. 2018;88:67–76.

[30] Criscenti G, Longoni A, Di Luca A, et al. Triphasic scaffolds for the regeneration of the bone–ligament interface. Biofabrication. 2016;8(1):015009.

[31] Kim WJ, Yun H-S, Kim GH. An innovative cell-laden α-TCP/collagen scaffold fabricated using a two-step printing process for potential application in regenerating hard tissues. Sci Rep. 2017;7(1):3181.

[32] Shim J-H, Lee J-S, Kim JY, et al. Bioprinting of a mechanically enhanced three-dimensional dual cell-laden construct for osteochondral tissue engineering using a multi-head tissue/organ building system. J Micromech Microeng. 2012;22(8):085014.

[33] Ozbolat IT, Hospodiuk M. Current advances and future perspectives in extrusion-based bioprinting. Biomaterials. 2016;76:321–343.

[34] Jakus AE, Rutz AL, Jordan SW, et al. Hyperelastic 'bone': a highly versatile, growth factor–free, osteoregenerative, scalable, and surgically friendly biomaterial. Sci Transl Med. 2016;8(358):358ra127–358ra127.

[35] Golafshan N, Vorndran E, Zaharievski S, et al. Tough magnesium phosphate-based 3D-printed implants induce bone regeneration in an equine defect model. Biomaterials. 2020;261:120302.

[36] Ahlfeld T, Doberenz F, Kilian D, et al. Bioprinting of mineralized constructs utilizing multichannel plotting of a self-setting calcium phosphate cement and a cell-laden bioink. Biofabrication. 2018;10 (4):045002.

[37] Shim J-H, Jang K-M, Hahn SK, et al. Three-dimensional bioprinting of multilayered constructs containing human mesenchymal stromal cells for osteochondral tissue regeneration in the rabbit knee joint. Biofabrication. 2016;8(1):014102.

[38] de Ruijter M, Ribeiro A, Dokter I, et al. Simultaneous micropatterning of fibrous meshes and bioinks for the fabrication of living tissue constructs. Adv Healthc Mater. 2019;8(7):1800418.

[39] Wei C, Dong J. Hybrid hierarchical fabrication of three-dimensional scaffolds. J Manuf Process. 2014;16(2):257–263.

[40] Castilho M, de Ruijter M, Beirne S, et al. Multitechnology biofabrication: a new approach for the manufacturing of functional tissue structures? Trends Biotechnol. 2020;38(12):1316–1328.

[41] Haider A, Haider S, Kummara MR, et al. Advances in the scaffolds fabrication techniques using biocompatible polymers and their biomedical application: a technical and statistical review. J Saudi Chem Soc. 2020;24(2):186–215.

[42] Bottino MC, Thomas V, Janowski GM. A novel spatially designed and functionally graded electrospun membrane for periodontal regeneration. Acta Biomater. 2011;7(1):216–224.

[43] Xue J, Wu T, Dai Y, et al. Electrospinning and electrospun nanofibers: methods, materials, and applications. Chem Rev. 2019;119(8):5298–5415.

[44] Uyar T, Kny E. Electrospun materials for tissue engineering and biomedical applications: research, design and commercialization. Woodhead Publishing; 2017;146–177.

[45] Yu X, Tang X, Gohil SV, et al. Biomaterials for bone regenerative engineering. Adv Healthc Mater. 2015;4 (9):1268–1285.

[46] Wu X, Miao L, Yao Y, et al. Electrospun fibrous scaffolds combined with nanoscale hydroxyapatite induce osteogenic differentiation of human periodontal ligament cells. Int J Nanomedicine. 2014;9:4135.

[47] Goncalves F, de Moraes MS, Ferreira LB, et al. Combination of bioactive polymeric membranes and stem cells for periodontal regeneration: in vitro and in vivo analyses. PLoS One. 2016;11(3): e0152412.

[48] Rowe MJ, Kamocki K, Pankajakshan D, et al. Dimensionally stable and bioactive membrane for guided bone regeneration: anin vitrostudy. J Biomed Mater Res B. 2016;104(3):594–605.

[49] Zhou T, Liu X, Sui B, et al. Development of fish collagen/bioactive glass/chitosan composite nanofibers as a GTR/GBR membrane for inducing periodontal tissue regeneration. Biomed Mater. 2017;12 (5):055004.

[50] Bottino MC, Arthur RA, Waeiss RA, et al. Biodegradable nanofibrous drug delivery systems: effects of metronidazole and ciprofloxacin on periodontopathogens and commensal oral bacteria. Clin Oral Investig. 2014;18(9):2151–2158.

[51] Wright ME, Wong AT, Levitt D, et al. Influence of ciprofloxacin-based additives on the hydrolysis of nanofiber polyurethane membranes. J Biomed Mater Res A. 2018;106(5):1211–1222.

[52] Münchow EA, Albuquerque MTP, Zero B, et al. Development and characterization of novel ZnO-loaded electrospun membranes for periodontal regeneration. Dent Mater. 2015;31(9):1038–1051.

[53] Furtos G, Rivero G, Rapuntean S, et al. Amoxicillin-loaded electrospun nanocomposite membranes for dental applications. J Biomed Mater Res B. 2017;105(5):966–976.

[54] Yar M, Farooq A, Shahzadi L, et al. Novel meloxicam releasing electrospun polymer/ceramic reinforced biodegradable membranes for periodontal regeneration applications. Mater Sci Eng: C. 2016;64:148–156.

[55] Kharaziha M, Fathi MH, Edris H, et al. PCL-forsterite nanocomposite fibrous membranes for controlled release of dexamethasone. J Mater Sci: Mater Med. 2015;26(1):36.

[56] Ranjbar-Mohammadi M, Zamani M, Prabhakaran M, et al. Electrospinning of PLGA/gum tragacanth nanofibers containing tetracycline hydrochloride for periodontal regeneration. Mater Sci Eng C. 2016;58:521–531.

[57] He M, Jiang H, Wang R, et al. Fabrication of metronidazole loaded poly (ε-caprolactone)/zein core/shell nanofiber membranes via coaxial electrospinning for guided tissue regeneration. J Colloid Interface Sci. 2017;490:270–278.

[58] Cheng G, Yin C, Tu H, et al. Controlled co-delivery of growth factors through layer-by-layer assembly of core–shell nanofibers for improving bone regeneration. ACS Nano. 2019;13(6):6372–6382.

[59] Yin L, Yang S, He M, et al. Physicochemical and biological characteristics of BMP-2/IGF-1-loaded three-dimensional coaxial electrospun fibrous membranes for bone defect repair. J Mater Sci: Mater Med. 2017;28(6):94.

[60] Ho M-H, Chang H-C, Chang Y-C, et al. PDGF-metronidazole-encapsulated nanofibrous functional layers on collagen membrane promote alveolar ridge regeneration. Int J Nanomedicine. 2017;12:5525–5535.

[61] Reise M, Wyrwa R, Müller U, et al. Release of metronidazole from electrospun poly(l-lactide-co-d/l-lactide) fibers for local periodontitis treatment. Dent Mater. 2012;28(2):179–188.

[62] He P, Zhong Q, Ge Y, et al. Dual drug loaded coaxial electrospun PLGA/PVP fiber for guided tissue regeneration under control of infection. Mater Sci Eng C. 2018;90:549–556.

[63] Shahi R, Albuquerque M, Münchow E, et al. Novel bioactive tetracycline-containing electrospun polymer fibers as a potential antibacterial dental implant coating. Odontology. 2017;105(3):354–363.

[64] Jia L-n, Zhang X, Xu H-y, et al. Development of a doxycycline hydrochloride-loaded electrospun nanofibrous membrane for GTR/GBR applications. J Nanomat. 2016;2016:1–10.

[65] Nasajpour A, Ansari S, Rinoldi C, et al. A multifunctional polymeric periodontal membrane with osteogenic and antibacterial characteristics. Adv Funct Mater. 2018;28(3):1703437.

[66] Nasajpour A, Mandla S, Shree S, et al. Nanostructured fibrous membranes with rose spike-like architecture. Nano Lett. 2017;17(10):6235–6240.

[67] Hokmabad VR, Davaran S, Aghazadeh M, et al. Fabrication and characterization of novel ethyl cellulose-grafted-poly (ε-caprolactone)/alginate nanofibrous/macroporous scaffolds incorporated with nano-hydroxyapatite for bone tissue engineering. J Biomater Appl. 2019;33(8):1128–1144.

[68] Ko E, Lee JS, Kim H, et al. Electrospun silk fibroin nanofibrous scaffolds with two-stage hydroxyapatite functionalization for enhancing the osteogenic differentiation of human adipose-derived mesenchymal stem cells. ACS Appl Mater Interfaces. 2018;10 (9):7614–7625.

[69] Wang Z, Liang R, Jiang X, et al. Electrospun PLGA/ PCL/OCP nanofiber membranes promote osteogenic differentiation of mesenchymal stem cells (MSCs). Mater. Sci. Eng. C. 2019;104:109796.

[70] Daghrery A, Aytac Z, Dubey N, et al. Electrospinning of dexamethasone/cyclodextrin inclusion complex polymer fibers for dental pulp therapy. Colloids Surf B. 2020: 111011.

[71] Liu W, Bi W, Sun Y, et al. Biomimetic organic-inorganic hybrid hydrogel electrospinning periosteum for accelerating bone regeneration. Mater Sci Eng C. 2020;110:110670.

[72] Aragón J, Salerno S, De Bartolo L, et al. Polymeric electrospun scaffolds for bone morphogenetic protein 2 delivery in bone tissue engineering. J Colloid Interface Sci. 2018;531:126–137.

[73] Wang Z, Wang Z, Lu WW, et al. Novel biomaterial strategies for controlled growth factor delivery for biomedical applications. NPG Asia Mater. 2017;9 (10):e435–e435.

[74] Kowalczewski CJ, Saul JM. Biomaterials for the delivery of growth factors and other therapeutic agents in tissue engineering approaches to bone regeneration. Front Pharmacol. 2018;9:513.

[75] Hutmacher DW, Dalton PD. Melt electrospinning. Chem–Asian J. 2011;6(1):44–56.

[76] Kade JC, Dalton PD. Polymers for melt electrowriting. Adv Healthc Mater. 2020;10(1):2001232.

[77] Peiffer QC, de Ruijter M, van Duijn J, et al. Melt electrowriting onto anatomically relevant biodegradable substrates: resurfacing a diarthrodial joint. Mater Des. 2020;195:109025.

[78] Abbasi N, Ivanovski S, Gulati K, et al. Role of offset and gradient architectures of 3-D melt electrowritten scaffold on differentiation and mineralization of osteoblasts. Biomater Res. 2020;24(1):2.

[79] Igawa K, Chung U, Tei Y. Custom-made artificial bones fabricated by an inkjet printing technology. Clin Calcium. 2008;18(12):1737.

[80] Atala A, Yoo JJ. Essentials of 3D biofabrication and translation. Cambridge: Academic Press; 2015.

[81] Placone JK, Engler AJ. Recent advances in extrusion-based 3D printing for biomedical applications. Adv Healthc Mater. 2018;7(8):1701161.

[82] Shim J-H, Kim SE, Park JY, et al. Three-dimensional printing of rhbmp-2-loaded scaffolds with long-term delivery for enhanced bone regeneration in a rabbit diaphyseal defect. Tissue Eng, Part A. 2014;20(13-14):1980–1992.

[83] Shim J-H, Yoon M-C, Jeong C-M, et al. Efficacy of rhBMP-2 loaded PCL/PLGA/β-TCP guided bone regeneration membrane fabricated by 3D printing technology for reconstruction of calvaria defects in rabbit. Biomed Mater. 2014;9(6):065006.

[84] Costa PF, Puga AM, Díaz-Gomez L, et al. Additive manufacturing of scaffolds with dexamethasone controlled release for enhanced bone regeneration. Int J Pharm. 2015;496(2):541–550.

[85] Won J, Park C, Bae J, et al. Evaluation of 3D printed PCL/PLGA/β-TCP versus collagen membranes for guided bone regeneration in a beagle implant model. Biomed Mater. 2016;11(5):055013.

[86] Kim G, Ahn S, Kim Y, et al. Coaxial structured collagen–alginate scaffolds: fabrication, physical properties, and biomedical application for skin tissue regeneration. J Mater Chem. 2011;21(17): 6165–6172.

[87] Malda J, Visser J, Melchels FP, et al. 25th anniversary article: engineering hydrogels for biofabrication. Adv Mater. 2013;25(36):5011–5028.

[88] Shim J-H, Jeong J-h, Won J-Y, et al. Porosity effect of 3D-printed polycaprolactone membranes on calvarial defect model for guided bone regeneration. Biomed Mater. 2018;13(1):015014.

[89] Wang M, Favi P, Cheng X, et al. Cold atmospheric plasma (CAP) surface nanomodified 3D printed polylactic acid (PLA) scaffolds for bone regeneration. Acta Biomater. 2016;46:256–265.

[90] Yu J, Xu Y, Li S, et al. Three-dimensional printing of nano hydroxyapatite/poly(ester urea) composite scaffolds with enhanced bioactivity. Biomacromolecules. 2017;18(12):4171–4183.

[91] Kwon DY, Park JH, Jang SH, et al. Bone regeneration by means of a three-dimensional printed scaffold in a rat cranial defect. J Tissue Eng Regen Med. 2018;12 (2):516–528.

[92] Park SH, Park SA, Kang YG, et al. PCL/β-TCP composite scaffolds exhibit positive osteogenic differentiation with mechanical stimulation. Tissue Eng Regen Med. 2017;14(4):349–358.

[93] Poh PS, Hutmacher DW, Holzapfel BM, et al. In vitro and in vivo bone formation potential of surface calcium phosphate-coated polycaprolactone and polycaprolactone/bioactive glass composite scaffolds. Acta Biomater. 2016;30:319–333.

[94] Cui H, Zhu W, Holmes B, et al. Biologically inspired smart release system based on 3D bioprinted perfused scaffold for vascularized tissue regeneration. Adv Sci. 2016;3(8):1600058.

[95] Vaquette C, Saifzadeh S, Farag A, et al. Periodontal tissue engineering with a multiphasic construct and cell sheets. J Dent Res. 2019;98(6):673–681.

[96] Lee CH, Hajibandeh J, Suzuki T, et al. Three-dimensional printed multiphase scaffolds for regeneration of periodontium complex. Tissue Eng, Part A. 2014;20(7-8):1342–1351.

[97] Muerza-Cascante ML, Shokoohmand A, Khosrotehrani K, et al. Endosteal-like extracellular matrix expression on melt electrospun written scaffolds. Acta Biomater. 2017;52:145–158.

[98] Hochleitner G, Kessler M, Schmitz M, et al. Melt electrospinning writing of defined scaffolds using polylactide-poly(ethylene glycol) blends with 45S5 bioactive glass particles. Mater Lett. 2017;205:257–260.

[99] Abdal-hay A, Abbasi N, Gwiazda M, et al. Novel polycaprolactone/hydroxyapatite nanocomposite fibrous scaffolds by direct melt-electrospinning writing. Eur Polym J. 2018;105:257–264.

[100] Hochleitner G, Chen F, Blum C, et al. Melt electrowriting below the critical translation speed to fabricate crimped elastomer scaffolds with non-linear extension behaviour mimicking that of ligaments and tendons. Acta Biomater. 2018;72:110–120.

[101] Baldwin J, Wagner F, Martine L, et al. Periosteum tissue engineering in an orthotopic in vivo platform. Biomaterials. 2017;121:193–204.

[102] Di Luca A, Ostrowska B, Lorenzo-Moldero I, et al. Ultrastructural characterization of the lower motor system in a mouse model of Krabbe disease. Sci Rep. 2016;6(1):1–13.

[103] Yang C, Wang X, Ma B, et al. 3D-Printed bioactive Ca_3SiO_5Bone cement scaffolds with nano surface structure for bone regeneration. ACS Appl Mater Interfaces. 2017;9(7):5757–5767.

[104] Martínez-Vázquez F, Cabañas M, Paris J, et al. Fabrication of novel Si-doped hydroxyapatite/gelatine scaffolds by rapid prototyping for drug delivery and bone regeneration. Acta Biomater. 2015;15:200–209.

[105] Luo G, Ma Y, Cui X, et al. 13-93 bioactive glass/alginate composite scaffolds 3D printed under mild conditions for bone regeneration. RSC Adv. 2017;7 (20):11880–11889.

[106] Zhao S, Zhang J, Zhu M, et al. Three-dimensional printed strontium-containing mesoporous bioactive glass scaffolds for repairing rat critical-sized calvarial defects. Acta Biomater. 2015;12:270–280.

[107] Fahimipour F, Dashtimoghadam E, Rasoulianboroujeni M, et al. Collagenous matrix supported by a 3D-printed scaffold for osteogenic differentiation of dental pulp cells. Dent Mater. 2018;34 (2):209–220.

[108] Liu A, Sun M, Yang X, et al. Three-dimensional printing akermanite porous scaffolds for load-bearing bone defect repair: An investigation of osteogenic capability and mechanical evolution. J Biomater Appl. 2016;31(5):650–660.

[109] Zhang W, Feng C, Yang G, et al. 3D-printed scaffolds with synergistic effect of hollow-pipe structure and bioactive ions for vascularized bone regeneration. Biomaterials. 2017;135:85–95.

[110] Feng C, Zhang W, Deng C, et al. 3D printing of lotus root-like biomimetic materials for cell delivery and tissue regeneration. Advanced Science. 2017;4 (12):1700401.

[111] Akkineni AR, Luo Y, Schumacher M, et al. 3D plotting of growth factor loaded calcium phosphate cement scaffolds. Acta Biomater. 2015;27:264–274.

[112] Fahimipour F, Rasoulianboroujeni M, Dashtimoghadam E, et al. 3D printed TCP-based scaffold incorporating VEGF-loaded PLGA microspheres for craniofacial tissue engineering. Dent Mater. 2017;33(11):1205–1216.

[113] Wang H, Wu G, Zhang J, et al. Osteogenic effect of controlled released rhBMP-2 in 3D printed porous hydroxyapatite scaffold. Colloids Surf B. 2016;141:491–498.

[114] Li C, Jiang C, Deng Y, et al. Ror2 signaling regulates Golgi structure and transport through IFT20 for tumor invasiveness. Sci Rep. 2017;7(1):1–12.

[115] Bekisz JM, Flores RL, Witek L, et al. Dipyridamole enhances osteogenesis of three-dimensionally printed bioactive ceramic scaffolds in calvarial defects. J Cranio-Maxillofacial Surg. 2018;46 (2):237–244.

[116] Luo Y, Zhai D, Huan Z, et al. Three-Dimensional Printing of hollow-struts-packed bioceramic scaffolds for bone regeneration. ACS Appl Mater Interfaces. 2015;7(43):24377–24383.

[117] Shao H, Sun M, Zhang F, et al. Custom repair of mandibular bone defects with 3D printed bioceramic scaffolds. J Dent Res. 2018;97(1):68–76.

[118] Lopez CD, Diaz-Siso JR, Witek L, et al. Three dimensionally printed bioactive ceramic scaffold osseoconduction across critical-sized mandibular defects. J Surg Res. 2018;223:115–122.

[119] Lai Y, Cao H, Wang X, et al. Porous composite scaffold incorporating osteogenic phytomolecule icariin for promoting skeletal regeneration in challenging osteonecrotic bone in rabbits. Biomaterials. 2018;153:1–13.

[120] Fedorovich NE, De Wijn JR, Verbout AJ, et al. Three-dimensional fiber deposition of cell-laden, viable, patterned constructs for bone tissue printing. Tissue Eng, Part A. 2008;14(1):127–133.

[121] Kim W, Kim G. Collagen/bioceramic-based composite bioink to fabricate a porous 3D hASCs-laden structure for bone tissue regeneration. Biofabrication. 2020;12(1):015007.

[122] Chimene D, Miller L, Cross LM, et al. Nanoengineered osteoinductive bioink for 3D bioprinting bone tissue. ACS Appl Mater Interfaces. 2020;12(14):15976–15988.

[123] Carlier A, Skvortsov GA, Hafezi F, et al. Computational model-informed design and bioprinting of cell-patterned constructs for bone tissue engineering. Biofabrication. 2016;8(2):025009.

[124] Lin HY, Chang TW, Peng TK. Three-dimensional plotted alginate fibers embedded with diclofenac and bone cells coated with chitosan for bone regeneration during inflammation. J Biomed Mater Res A. 2018;106(6):1511–1521.

[125] Maliha SG, Lopez CD, Coelho PG, et al. Bone tissue engineering in the growing calvaria using dipyridamole-coated, three-dimensionally-printed bioceramic scaffolds. Plast Reconstr Surg. 2020;145 (2):337e.

[126] Pilipchuk SP, Monje A, Jiao Y, et al. Integration of 3D printed and micropatterned polycaprolactone scaffolds for guidance of oriented collagenous tissue formation In vivo. Adv Healthc Mater. 2016;5 (6):676–687.

[127] Gómez-Cerezo N, Casarrubios L, Saiz-Pardo M, et al. Mesoporous bioactive glass/ε-polycaprolactone scaffolds promote bone regeneration in osteoporotic sheep. Acta Biomater. 2019;90:393–402.

[128] Feng X, Wu Y, Bao F, et al. Comparison of 3D-printed mesoporous calcium silicate/polycaprolactone and mesoporous bioactive glass/polycaprolactone scaffolds for bone regeneration. Microporous Mesoporous Mater. 2019;278:348–353.

[129] Lee J, Farag MM, Park EK, et al. A simultaneous process of 3D magnesium phosphate scaffold fabrication and bioactive substance loading for hard tissue regeneration. Mater Sci Eng C. 2014;36:252–260.

[130] Gbureck U, Hölzel T, Klammert U, et al. Resorbable dicalcium phosphate bone substitutes prepared by 3D powder printing. Adv Funct Mater. 2007;17 (18):3940–3945.

[131] Castilho M, Dias M, Vorndran E, et al. Application of a 3D printed customized implant for canine cruciate ligament treatment by tibial tuberosity advancement. Biofabrication. 2014;6(2):025005.

[132] Diloksumpan P, de Ruijter M, Castilho M, et al. Combining multi-scale 3D printing technologies to engineer reinforced hydrogel-ceramic interfaces. Biofabrication. 2020;12(2):025014.

[133] Deng Y, Jiang C, Li C, et al. Ror2 signaling regulates Golgi structure and transport through IFT20 for tumor invasiveness. Sci Rep. 2017;7(1):1–14.

[134] Subbiah R, Hipfinger C, Tahayeri A, et al. 3D printing of microgel-loaded modular microcages as instructive scaffolds for tissue engineering. Adv Mater. 2020;32(36):2001736.

[135] Wang MM, Flores RL, Witek L, et al. Dipyridamole-loaded 3D-printed bioceramic scaffolds stimulate pediatric bone regeneration in vivo without disruption of craniofacial growth through facial maturity.. Sci Rep. 2019;9(1):1–15.

[136] Park CH, Kim K-H, Lee Y-M, et al. 3D printed, microgroove pattern-driven generation of oriented ligamentous architectures. Int J Mol Sci. 2017;18(9):1927.

[137] Witek L, Alifarag AM, Tovar N, et al. Repair of critical-sized long bone defects using dipyridamole-augmented 3D-printed bioactive ceramic scaffolds. J Orthop Res. 2019;37(12):2499–2507.

[138] Zhang M, Lin R, Wang X, et al. 3D printing of Haversian bone–mimicking scaffolds for multicellular delivery in bone regeneration. Sci Adv. 2020;6(12):eaaz6725.

[139] Vorndran E, Klammert U, Ewald A, et al. Simultaneous immobilization of bioactives during 3D powder printing of bioceramic drug-release matrices. Adv Funct Mater. 2010;20(10):1585–1591.

[140] Yan Y, Chen H, Zhang H, et al. Vascularized 3D printed scaffolds for promoting bone regeneration. Biomaterials. 2019;190:97–110.

[141] Crump SS. Apparatus and method for creating three-dimensional objects. 1992, Google Patents.

[142] Youssef A, Hollister SJ, Dalton PD. Additive manufacturing of polymer melts for implantable medical devices and scaffolds. Biofabrication. 2017;9(1):012002.

[143] Ngo TD, Kashani A, Imbalzano G, et al. Additive manufacturing (3D printing): a review of materials, methods, applications and challenges. Compos B: Eng. 2018;143:172–196.

[144] Hong JM, Kim BJ, Shim J-H, et al. Enhancement of bone regeneration through facile surface functionalization of solid freeform fabrication-based three-dimensional scaffolds using mussel adhesive proteins. Acta Biomater. 2012;8(7):2578–2586.

[145] Mwema FM, Akinlabi ET. 'Basics of fused deposition modelling (FDM)', in 'Fused deposition modeling', 1–15; 2020, Springer.

[146] Kim K, Lee C, Kim B, et al. Anatomically shaped tooth and periodontal regeneration by cell homing. J Dent Res. 2010;89(8):842–847.

[147] Oladapo BI, Zahedi S, Adeoye A. 3D printing of bone scaffolds with hybrid biomaterials. Compos B: Eng. 2019;158:428–436.

[148] Goncalves EM, Oliveira FJ, Silva RF, et al. Three-dimensional printed PCL-hydroxyapatite scaffolds filled with CNTs for bone cell growth stimulation. J Biomed Mater Res B: Appl Biomater. 2016;104(6):1210–1219.

[149] Vaquette C, Fan W, Xiao Y, et al. A biphasic scaffold design combined with cell sheet technology for simultaneous regeneration of alveolar bone/periodontal ligament complex. Biomaterials. 2012;33(22):5560–5573.

[150] Dalton PD. Melt electrowriting with additive manufacturing principles. Curr Opin Biomed Eng. 2017;2:49–57.

[151] Abbasi N, Abdal-Hay A, Hamlet S. Effects of gradient and offset architectures on the mechanical and biological properties of 3-D melt electrowritten (MEW) scaffolds. ACS Biomater Sci Eng. 2019;5:3448–3461.

[152] Visser J, Melchels FP, Jeon JE, et al. Reinforcement of hydrogels using three-dimensionally printed microfibres. Nat Commun. 2015;6(1):1–10.

[153] Castilho M, Mouser V, Chen M, et al. Bi-layered micro-fibre reinforced hydrogels for articular cartilage regeneration. Acta Biomater. 2019;95:297–306.

[154] Gu Z, Fu J, Lin H, et al. Development of 3D bioprinting: from printing methods to biomedical applications. Asian J Pharm Sci. 2019;15(5):529–557.

[155] Vozzi G, Flaim CJ, Bianchi F, et al. Microfabricated PLGA scaffolds: a comparative study for application to tissue engineering. Mater Sci Eng C. 2002;20(1-2):43–47.

[156] Hospodiuk M, Dey M, Sosnoski D, et al. The bioink: A comprehensive review on bioprintable materials. Biotechnol Adv. 2017;35(2):217–239.

[157] Du X, Fu S, Zhu Y. 3D printing of ceramic-based scaffolds for bone tissue engineering: an overview. J Mater Chem B. 2018;6(27):4397–4412.

[158] He Y, Yang F, Zhao H, et al. Research on the printability of hydrogels in 3D bioprinting. Sci Rep. 2016;6:29977.

[159] Labate GFDU, Catapano G, Vitale-Brovarone C, et al. Quantifying the micro-architectural similarity of bioceramic scaffolds to bone. Ceram Int. 2017;43(12):9443–9450.

[160] Christel T, Kuhlmann M, Vorndran E, et al. Dual setting α-tricalcium phosphate cements. J Mater Sci: Mater Med. 2013;24(3):573–581.

[161] Castilho M, Moseke C, Ewald A, et al. Direct 3D powder printing of biphasic calcium phosphate scaffolds for substitution of complex bone defects. Biofabrication. 2014;6(1):015006.

[162] De Witte T-M, Fratila-Apachitei LE, Zadpoor AA, et al. Bone tissue engineering via growth factor delivery: from scaffolds to complex matrices. Regen Biomater. 2018;5(4):197–211.

[163] Feng C, Zhang M, Bhandari B. Materials properties of printable edible inks and printing parameters Optimization during 3D printing: a review. Crit Rev Food Sci Nutr. 2019;59(19):3074–3081.

[164] Parent M, Baradari H, Champion E, et al. Design of calcium phosphate ceramics for drug delivery applications in bone diseases: a review of the parameters affecting the loading and release of the therapeutic substance. J Controlled Release. 2017;252:1–17.

[165] Paul W, Sharma CP. Ceramic drug delivery: a perspective. J Biomater Appl. 2003;17(4):253–264.

[166] Cao X, Chen D. The BMP signaling and in vivo bone formation. Gene. 2005;357(1):1–8.

[167] Groll J, Boland T, Blunk T, et al. Biofabrication: reappraising the definition of an evolving field. Biofabrication. 2016;8(1):013001.

[168] Murphy SV, Atala A. 3D bioprinting of tissues and organs. Nat Biotechnol. 2014;32(8):773–785.

[169] Möller T, Amoroso M, Hägg D, et al. In vivo chondrogenesis in 3D bioprinted human cell-laden hydrogel constructs. Plast Reconstr Surg Glob Open. 2017;5(2).

[170] Groll J, Burdick JA, Cho D-W, et al. A definition of bioinks and their distinction from biomaterial inks. Biofabrication. 2019;11(1):013001.

[171] Tibbitt MW, Anseth KS. Hydrogels as extracellular matrix mimics for 3D cell culture. Biotechnol Bioeng. 2009;103(4):655–663.

[172] Zhang H-B, Xing T-L, Yin R-X, et al. Three-dimensional bioprinting is not only about cell-laden structures. Chin J Traumatol. 2016;19(4):187–192.

[173] Asa'ad F, Pagni G, Pilipchuk SP, et al. 3D-Printed scaffolds and biomaterials: review of alveolar bone augmentation and periodontal regeneration applications. Int J Dent. 2016: 2016:1239842.

[174] Swetha S, Lavanya K, Sruthi R, et al. An insight into cell-laden 3D-printed constructs for bone tissue engineering. J Mater Chem B. 2020;8(43): 9836–9862.

[175] Sadat-Shojai M, Khorasani M-T, Jamshidi A. 3-Dimensional cell-laden nano-hydroxyapatite/protein hydrogels for bone regeneration applications. Mater Sci Eng C. 2015;49:835–843.

[176] James AW, LaChaud G, Shen J, et al. A review of the clinical side effects of bone morphogenetic protein-2. Tissue Eng B: Rev. 2016;22(4):284–297.

[177] Xu T, Binder KW, Albanna MZ, et al. Hybrid printing of mechanically and biologically improved constructs for cartilage tissue engineering applications. Biofabrication. 2013;5(1):015001.

[178] Costa PF, Vaquette C, Zhang Q, et al. Advanced tissue engineering scaffold design for regeneration of the complex hierarchical periodontal structure. J Clin Periodontol. 2014;41(3):283–294.

[179] Hinton TJ, Jallerat Q, Palchesko RN, et al. Three-dimensional printing of complex biological structures by freeform reversible embedding of suspended hydrogels. Sci Adv. 2015;1(9):e1500758.

[180] Durmus NG, Tekin HC, Guven S, et al. Magnetic levitation of single cells. Proc Natl Acad Sci USA. 2015;112(28):E3661–E3668.

[181] Betsch M, Cristian C, Lin YY, et al. Incorporating 4D into bioprinting: real-time magnetically directed collagen fiber alignment for generating complex multilayered tissues. Adv Healthc Mater. 2018;7 (21):1800894.

[182] Liu F, Wang W, Mirihanage W, et al. A plasma-assisted bioextrusion system for tissue engineering. CIRP Ann. 2018;67(1):229–232.

[183] Wüst S, Müller R, Hofmann S. Controlled positioning of cells in biomaterials – approaches towards 3D tissue printing. J Funct Biomater. 2011;2(3):119–154.

[184] Ma L, Wang X, Zhao N, et al. Integrating 3D printing and biomimetic mineralization for personalized enhanced osteogenesis, angiogenesis, and osteointegration. ACS Appl Mater Interfaces. 2018;10(49):42146–42154.

[185] Li Y, Bai Y, Pan J, et al. A hybrid 3D-printed aspirin-laden liposome composite scaffold for bone tissue engineering. J Mater Chem B. 2019;7(4):619–629.

[186] Park CH, Rios HF, Taut AD, et al. Image-based, fiber guiding scaffolds: a platform for regenerating tissue interfaces. Tissue Eng C: Methods. 2014;20 (7):533–542.

[187] Park C, Kim K, Rios H, et al. Spatiotemporally controlled microchannels of periodontal mimic scaffolds. J Dent Res. 2014;93(12):1304–1312.